HADRON PRODUCTION BY NEUTRINOS ON PROTONS*

By N. Schmitz

Max-Planck-Institut für Physik und Astrophysik, München**
Aachen-Bonn-CERN-München(MPI)-Oxford Collaboration

(Received July 12, 1980)

In a bubble chamber experiment with BEBC filled with hydrogen at the CERN SPS the hadronic final state in neutrino-proton scattering has been studied by the Aachen-Bonn--CERN-München(MPI)-Oxford Collaboration. Results are presented on the following topics: charged multiplicity distribution, forward and backward multiplicities and charge distribution, production of neutral strange particles and of charm, quark-singlet and gluon fragmentation moments, non-factorisation and double moments, transverse momentum and jet studies.

PACS numbers: 13.15.+g

Introduction

In these lectures some recent results are discussed on the hadronic final state produced in charged-current (CC) neutrino-proton reactions

$$\nu_\mu p \to \mu^- + \text{hadrons}, \tag{1}$$

which were studied by the Aachen-Bonn-CERN-München (MPI)-Oxford Collaboration in a bubble chamber experiment (WA21) using BEBC filled with liquid hydrogen and exposed to a wide-band neutrino beam produced by protons of 350 GeV from the CERN SPS. Fig. 1 shows the neutrino-energy spectrum of the experiment, peaking at $E_\nu \approx 20$ GeV. Fig. 2 gives a side view and a top view of BEBC together with the two-plane external muon identifier (EMI) [1] which consists of an inner plane with 6 and an outer plane with 49 3m × 1m multiwire proportional chambers (covering an area of 150 m^2) and which allows the identification of the secondary muon with an efficiency of $\sim 98.5\%$ for $p_\mu > 10$ GeV/c and of $\sim 85\%$ on the average between 3 and 10 GeV/c. A correction for losses due to EMI inefficiencies was applied.

---

* Presented at the XX Cracow School of Theoretical Physics, Zakopane, May 29 — June 11, 1980.

** Address: Max-Planck-Institut für Physik und Astrophysik, Föhringer Ring 6, 8000 München 40, West Germany.

In a total of 285000 pictures, taken between August and December 1977 and corresponding to 1.1×10^{18} protons on the target, some 18000 events were measured on film plane digitizers, leading to ~7800 CC events with visible energy $E_{vis} > 5$ GeV and muon momentum $p_\mu > 3$ GeV/c in a fiducial volume of 18.9 m^3 corresponding to 1.1 tons of H_2. The magnetic field in the chamber was 3.5 Tesla. The measurements were processed by the CERN-HYDRA programs for geometry, kinematics and EMI, and particle identifi-

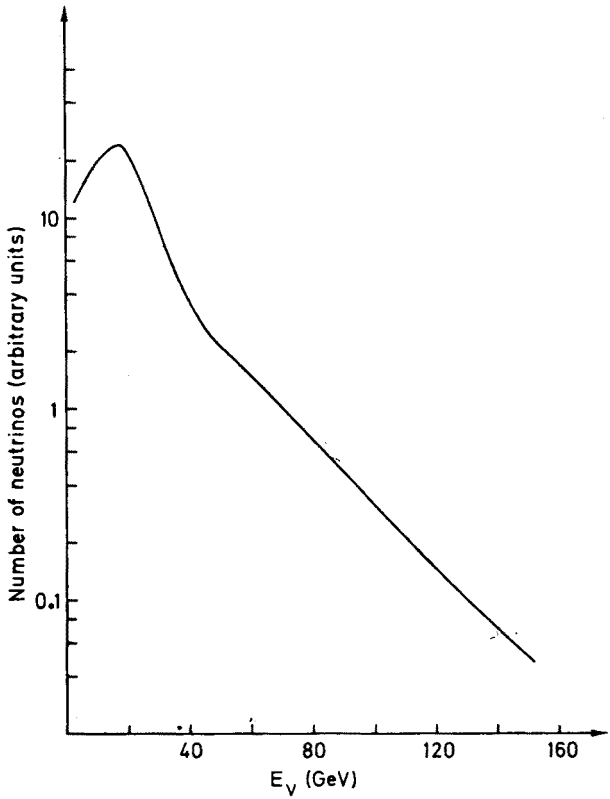

Fig. 1. Energy distribution of incident neutrinos in the BEBC experiment WA21

cation was performed, whenever possible, using energy loss (mass-dependent geometry), range and ionisation, and kinematical fits. For each event an estimate for the unmeasured neutrino lab energy E_ν was determined from estimating the total lab energy of all secondary hadrons (including unmeasured neutrals) by the following formula [2], which is based on transverse momentum balance:

$$E_{\mathrm{Hcorr}} = E_{\mathrm{Hvis}}\left(1 + \frac{|\vec{p}_{\mathrm{T}\mu} + \Sigma\vec{p}_{\mathrm{Ti}}|}{\Sigma|\vec{p}_{\mathrm{Ti}}|}\right), \qquad E_\nu = E_\mu + E_{\mathrm{Hcorr}} - M. \tag{2}$$

Here $\vec{p}_{\mathrm{T}\mu}$ and $\vec{p}_{\mathrm{Ti}}$ is the transverse momentum of the muon and of the ith observed (charged) hadron respectively, with respect to the known beam direction; E_{Hvis} is the lab energy of

all measured (charged) hadrons. This formula of estimating the neutrino energy differs somewhat from the usually applied transverse-momentum-balance method [3], but has been shown by Monte-Carlo simulations to lead to rather reliable and unbiased results. The neutrino-energy distribution of the events ranges from ~5 GeV to ~200 GeV, peaks at ~20 GeV and has an average of $\langle E_\nu \rangle \approx 42$ GeV.

Results from the experiment have been obtained and published so far on the following subjects: Production of charmed particles [4], Q^2 dependence of fragmentation functions and non-factorisation of semi-inclusive cross sections [5], ratio of neutral-to-charged current

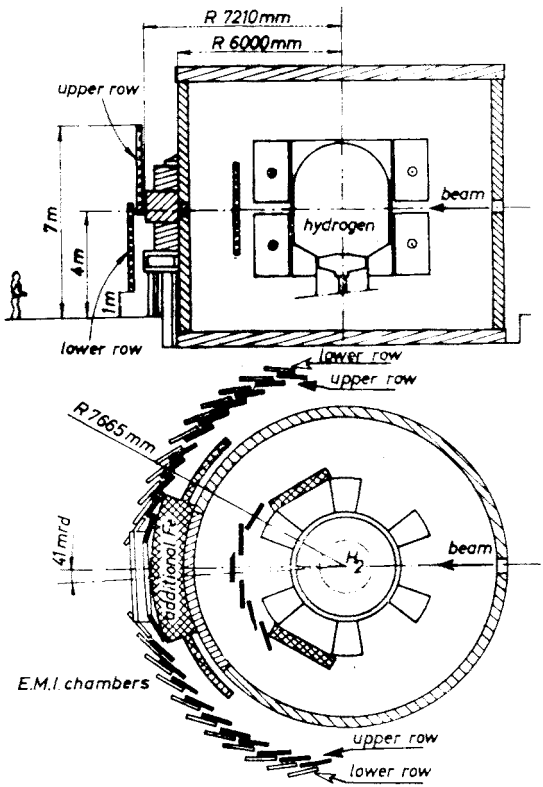

Fig. 2. Side view and top view of the Big European Bubble Chamber BEBC together with the two-plane External Myon Identifier EMI

cross sections [6], multiplicity distribution of charged hadrons [7], single π^+ and Δ^{++} production [8], charge distributions and total hadronic forward charge [9]. Results from the experiment can also be found in reviews given at the various conferences in 1979 [10–13]. In these lectures new results will be presented on the following topics without going into the details of experimental analysis:

A. Multiplicity distribution of charged hadrons

B. Forward and backward multiplicities, charge distribution

C. Production of neutral strange particles, charm production
D. Moments of quark-singlet and gluon fragmentation functions
E. Non-factorisation and double moments
F. Transverse momentum and jet studies.

A. Multiplicity distribution of charged hadrons

High-energy reactions can be subdivided into two classes A and B depending on whether diffractive scattering contributes or not:

class A: annihilation-like processes like $p\bar{p}$ or e^+e^- annihilation into hadrons, to which diffraction dissociation of one or both incident particles does not contribute.

class B: normal inclusive hadron-hadron collisions or (via the vector-meson dominance model) photoproduction, to which diffraction scattering contributes.

The multiplicity distribution of a class-B process is thought to consist of two components (two-component model, see e.g. Ref. [14]): a diffractive component which has low multiplicities n rather independent of energy, and a non-diffractive component with multiplicities moving towards higher values as the energy increases. The overall multiplicity distribution widens therefore with increasing energy and is expected to develop two visible parts with a valley in between at extremely large energies. A class-A process on the other hand has a narrower multiplicity distribution which moves towards higher n-values with increasing energy.

The interesting question arises: Which class does neutrino-nucleon scattering (1) belong to? This process is sketched in Fig. 3 where at the lower vertex the exchanged

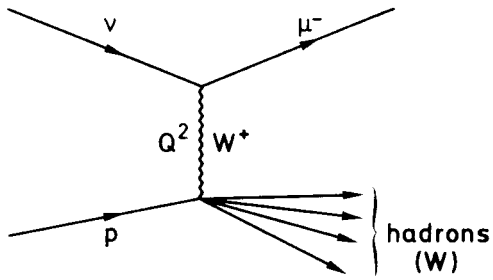

Fig. 3. Diagram for the reaction $\nu p \to \mu^- +$ hadrons

vector-boson W^+ interacts with the proton leading to the final-state hadrons:

$$W^+ p \to \text{hadrons}. \tag{3}$$

The effective mass W of all final-state hadrons (including neutrals) in reaction (1), i.e. the total cms energy of reaction (3) is given by

$$W^2 = M^2 + 2Mv - Q^2 \quad (v = E_\nu - E_\mu) \tag{4}$$

where

$$Q^2 = 4E_\mu E_\nu \sin^2 \frac{\theta}{2} \tag{5}$$

is the four-momentum transfer squared between incoming ν and outgoing μ with lab energies E_ν, E_μ and a lab angle θ between them.

In Fig. 4 the normalized topological cross sections $P(n, W) = \sigma(n, W)/\sigma_{tot}(W)$ are plotted vs W^2 for various charged hadron multiplicities n. From this figure the charged

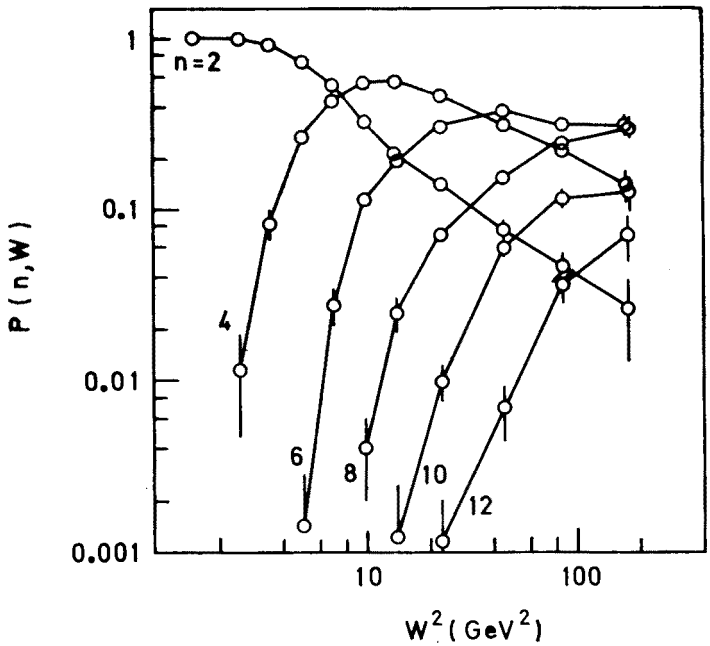

Fig. 4. Normalized topological νp cross sections $P(n, W) = \sigma(n, W)/\sigma_{tot}(W)$ vs W^2 for charged hadron multiplicities $n = 2, \ldots 12$. The curves are drawn to guide the eye

multiplicity distribution $P(n, W)$ at fixed W is of course directly obtained. One notices a strong decrease of $P(2)$ and (at higher W) also of $P(4)$ with W which indicates already the smallness of a diffractive component.

Fig. 5 shows the average charged multiplicity as a function of W^2; the experimental points above $W^2 = 4\,\mathrm{GeV}^2$ are well described by a fit linear in $\ln W^2$ yielding

$$\langle n \rangle = (0.37 \pm 0.02) + (1.33 \pm 0.02) \ln W^2, \quad (W \text{ in GeV}). \tag{6}$$

In contrast to the strong dependence on W, $\langle n \rangle$ is rather independent of Q^2 at fixed W. This is seen in Fig. 6, where even for a larger W interval ($4 < W < 10$ GeV) there is only little variation of $\langle n \rangle$ with Q^2.

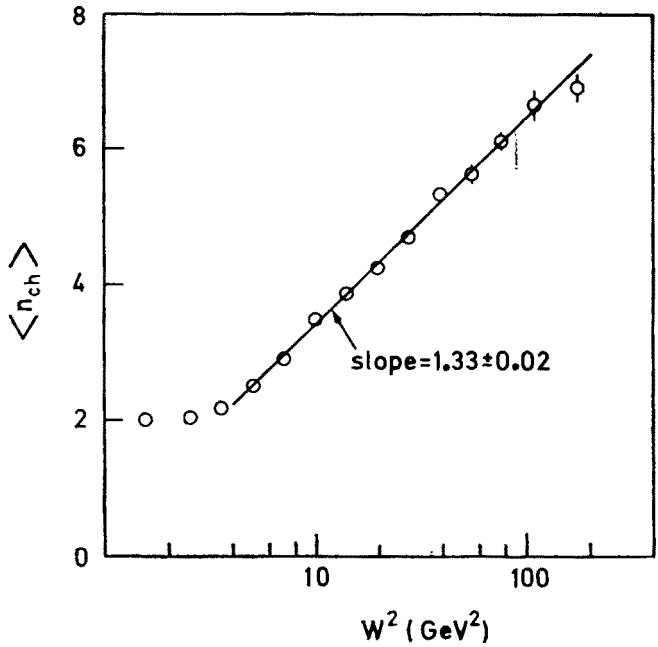

Fig. 5. Average charged multiplicity in νp scattering vs W^2. The curve is a fit of the form $\langle n \rangle = a + b \ln W^2$ for $W^2 > 4\,\mathrm{GeV}^2$

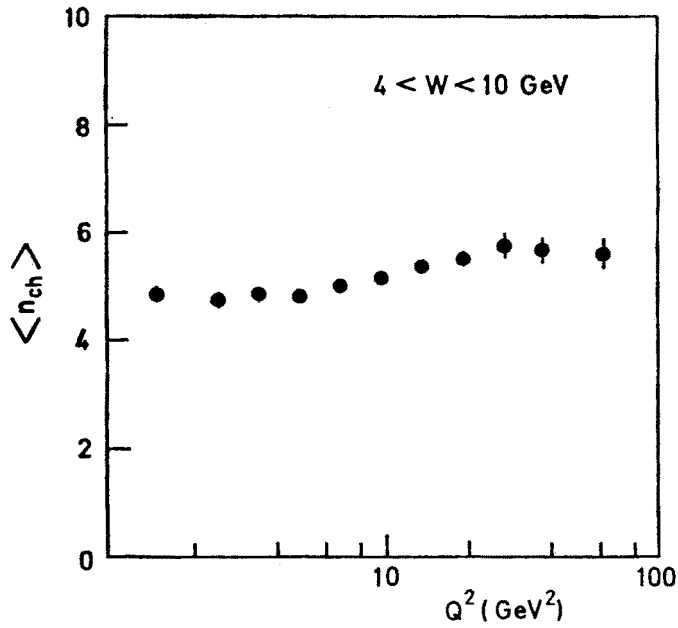

Fig. 6. Average charged multiplicity in νp scattering vs Q^2 for $4 < W < 10\,\mathrm{GeV}$

We now discuss the next-higher moments of the multiplicity distribution, namely the dispersion

$$D = \sqrt{\langle n^2\rangle - \langle n\rangle^2} \tag{7}$$

and the correlation parameter

$$f_2 = \langle n(n-1)\rangle - \langle n\rangle^2 = D^2 - \langle n\rangle \tag{8}$$

and compare the results of this experiment with those for $p\bar{p}$ annihilation (class A) and pp scattering (class B) [15–19]. Using the relation

$$n = \alpha + \beta n_- \tag{9}$$

between the multiplicity n_- of negative hadrons and the multiplicity n of charged hadrons, one obtains the relation

$$D_- \equiv \sqrt{\langle n_-^2\rangle - \langle n_-\rangle^2} = \frac{1}{\beta} D \tag{10}$$

between the dispersion D_- of the negative multiplicity distribution and the dispersion D of the charged multiplicity distribution, where

$$\begin{aligned} &\alpha = 2, \quad \beta = 2 \quad \text{for pp, vp} \\ &\alpha = 0, \quad \beta = 2 \quad \text{for } p\bar{p} \text{ annihilation.} \end{aligned} \tag{11}$$

An empirical linear relation of the form

$$D = a + b\langle n\rangle \tag{12}$$

has been found between D and $\langle n\rangle$ by Wróblewski [14] which for large $\langle n\rangle$ leads to a constant ratio

$$\frac{\langle n\rangle}{D} \xrightarrow[\langle n\rangle \to \infty]{} \frac{1}{b}. \tag{13}$$

The following values for the parameters a and b were obtained from fits to the data:

$$\begin{aligned} &D = 0.58(\langle n\rangle - 0.97) \quad \text{for pp scattering [19],} \\ &D = 0.37\langle n\rangle \quad \text{for } p\bar{p} \text{ annihilation [16].} \end{aligned} \tag{14}$$

Transforming this into D_- and $\langle n_-\rangle$ by using (9), (10) and (11) one obtains $\left(a_- = \frac{1}{\beta}(a + \alpha b),\ b_- = b\right)$

$$\begin{aligned} D_- &= a_- + b_-\langle n_-\rangle = 0.30 + 0.58\langle n_-\rangle \quad \text{for pp scattering,} \\ &= 0.37\langle n_-\rangle \quad \text{for } p\bar{p} \text{ annihilation.} \end{aligned} \tag{15}$$

These two straight lines representing the experimental data on pp and $p\bar{p}$ are shown in

Fig. 7 together with the experimental points from this experiment. It is seen that also the vp points fall on a straight line for $\langle n_- \rangle \gtrsim 0.5$, a linear fit yielding

$$D_- = (0.36 \pm 0.03) + (0.36 \pm 0.03)\,\langle n_- \rangle \tag{16}$$

(straight line through data points). Thus the asymptotic $\langle n \rangle / D$ ratio (Eq. (13)) is the same for vp and $p\bar{p}$ annihilation, whereas that for pp scattering is smaller.

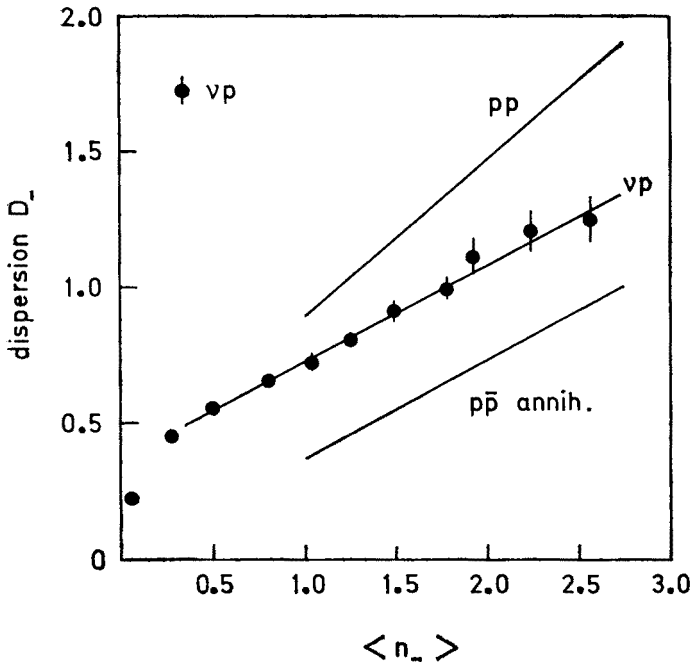

Fig. 7. Dispersion D_- of the multiplicity distribution of negative hadrons vs average multiplicity $\langle n_- \rangle$ of negative hadrons. The straight line through the data points for vp scattering is a fit of the form $D_- = a_- + b_- \langle n_- \rangle$. Shown are also the straight-line fits to the experimental results for pp scattering [19] and $p\bar{p}$ annihilation [16]

The linear relation (12), (15) leads to the following quadratic relation for the correlation parameter f_2^{--} (Eq. (8)) between negative hadrons as a function of $\langle n_- \rangle$:

$$f_2^{--} = D_-^2 - \langle n_- \rangle = a_-^2 + (2a_- b_- - 1)\,\langle n_- \rangle + b_-^2 \langle n_- \rangle^2. \tag{17}$$

Inserting the experimental values (15), (16) for the parameters a_-, b_- one obtains:

$$\begin{aligned} f_2^{--} &= 0.09 - 0.65\langle n_- \rangle + 0.34\langle n_- \rangle^2 && \text{for pp scattering,} \\ f_2^{--} &= -\langle n_- \rangle + 0.14\langle n_- \rangle^2 && \text{for } p\bar{p} \text{ annihilation,} \\ f_2^{--} &= 0.13 - 0.74\langle n_- \rangle + 0.13\langle n_- \rangle^2 && \text{for vp scattering.} \end{aligned} \tag{18}$$

These three relations are shown by the full curves in Fig. 8 together with the data points from this experiment. As expected, the predicted curve for vp scattering is in very good agreement with the experimental results. The dotted straight line is a direct linear fit[1] $f_2^{--} \approx -0.73\langle n_- \rangle$ [20] to the experimental $p\bar{p}$ data; it is closely approximated by the prediction (18) for $p\bar{p}$ (full curve). Again, the vp data points are much closer to the $p\bar{p}$ than to the pp results, the difference between vp and $p\bar{p}$ annihilation being probably due (as in Fig. 7) to the fact that in vp scattering the hadronic system has total charge 2 ($\alpha = 2$ in (11)), whereas it has charge 0 in $p\bar{p}$ annihilation.

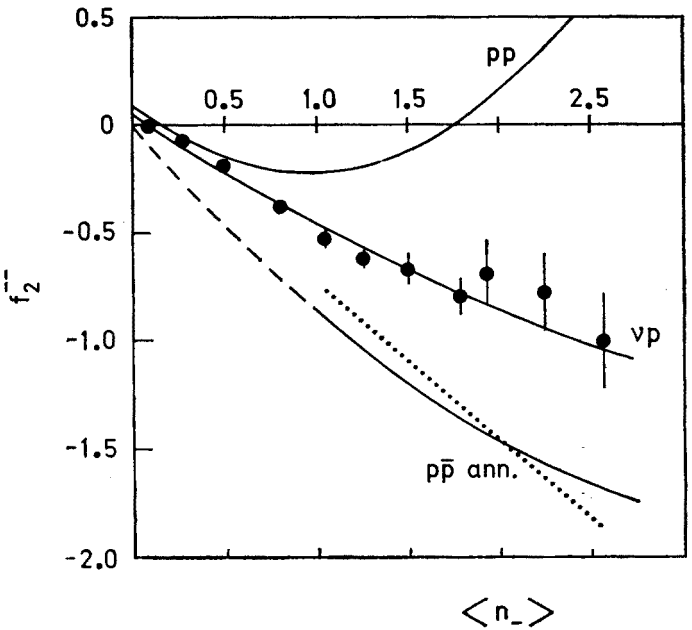

Fig. 8. Correlation parameter f_2^{-} vs average negative multiplicity in vp scattering. The full curves follow from the fits $D_- = a_- + b_- \langle n_- \rangle$ to the vp, pp and $p\bar{p}$ data for D_- vs $\langle n_- \rangle$. The dashed curve is a direct fit of the form $f_2^{-} = c\langle n_- \rangle$ [20]

Fig. 9 shows the scaled charged multiplicity distribution $\langle n \rangle P(n, W)$ vs. the normalized charged multiplicity $n/\langle n \rangle$ for five intervals of the hadronic mass W for reaction (3). It is seen that the points for various W fall on the same universal curve, which means that Koba-Nielsen-Olesen (KNO) scaling [21] is approximately fulfilled. The figure also shows the KNO scaling curves for pp scattering (full curve) and $p\bar{p}$ annihilation (dotted curve). The good agreement between vp scattering and $p\bar{p}$ annihilation strongly suggests that vp scattering is a class-A process (without diffraction scattering) whereas the KNO curve for pp scattering (class-B) is much wider as a consequence of the fact that diffractive scattering contributes as explained at the beginning of this section.

[1] Such a linear relation between f_2^{-} and $\langle n_- \rangle$ is of course not strictly compatible with the definition (17) of f_2^{-} and a linear relation (15) between D_- and $\langle n_- \rangle$.

Summarising one may conclude from the similarity between νp scattering and $p\bar{p}$ annihilation as observed in Figs. 7, 8, 9 that diffraction scattering does not contribute noticeably to νp scattering.

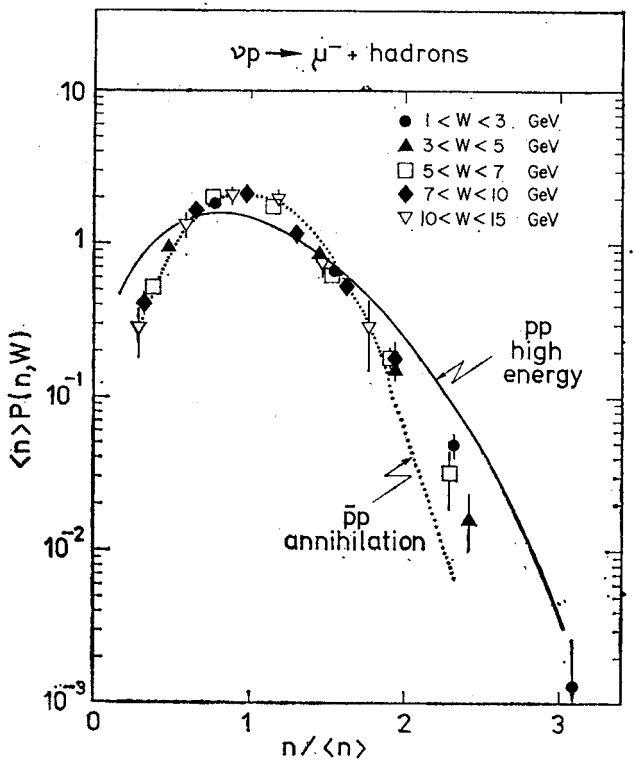

Fig. 9. KNO scaling distribution $\langle n\rangle P(n, W)$ vs $n/\langle n\rangle$ for five intervals of W for νp scattering. Shown are also the KNO curves to the data of high energy pp scattering and $p\bar{p}$ annihilation

B. Forward and backward multiplicities, charge distribution

According to the quark-parton model (QPM) which is sketched for νp scattering in Fig. 10, the hadrons in reaction (1) are produced in the following way: A d-quark of the proton absorbs the current (i.e. the intermediate vector boson W^+) and is thereby converted into a u-quark which subsequently fragments into the (forward going) current fragments. The two u-quarks of the proton (diquark system) are not involved in the interaction (spectator quarks) and fragment into the (backward going) target fragments. In order to separate (at least approximately) the two fragmentation regions from each other one usually subdivides the final-state hadrons into those going forward (i.e. in current direction) in the hadronic cm system (Feynman-$x_F = 2p^*_{\|}/W > 0$; current fragments) and those going backward ($x_F < 0$; target fragments). Of course, at small values of the hadronic mass W a strong kinematical overlap of the two types of fragments is expected, whereas

one may hope the x_F cut to become more and more efficient and meaningful, as W increases. This may be seen from Fig. 11a and b where the average number of positive and negative hadrons per event and per unit rapidity interval is plotted vs. rapidity in the hadronic cms

$$y = \tfrac{1}{2} \ln \frac{E^* + p_\parallel^*}{E^* - p_\parallel^*} \tag{19}$$

for two intervals of low and high W: Whereas at low W the rapidity distribution is quite narrow and peaked, the distribution (at least for the positive hadrons) starts to develop a plateau at high W which separates the two fragmentation regions.

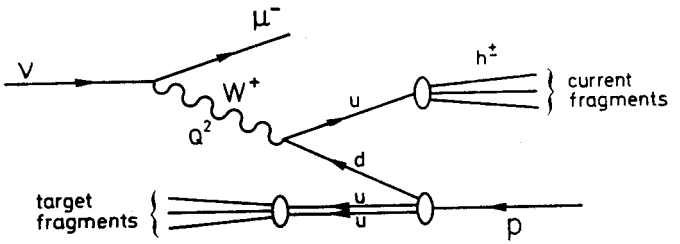

Fig. 10. Diagram of the quark-parton model for neutrinoproduction $\nu p \to \mu^- +$ hadrons

In Fig. 12 the average charged multiplicity $\langle n \rangle_{F,B}$ in the forward and backward hemispheres is plotted vs. W^2. The forward multiplicity is seen to be larger than the backward multiplicity for all W^2. In the QPM, this implies different fragmentation properties for the u-quark and for the diquark system. In Fig. 13 the forward and backward multiplicities of Fig. 12 are subdivided into their contributions from positive and negative hadrons. It is seen that at small W the forward-to-backward excess is due to positive hadrons whereas the average number of negative hadrons is nearly equal in the two hemispheres. At high W on the other hand, the situation is just reversed: There are more negative hadrons going forward than going backward, whereas the average numbers of positives become roughly equal in the two hemispheres. Another way of presenting this result is in terms of the average forward ($x_F > 0$) or backward ($x_F < 0$) going charge

$$\langle Q \rangle_{F,B} = \langle n_+ \rangle_{F,B} - \langle n_- \rangle_{F,B} \tag{20}$$

per event which is shown in Fig. 14 for the two hemispheres[2] as a function of W^2: For small W there is an excess ($\langle Q \rangle_F > 1$) of (positive) charge in the forward hemisphere whereas for large W more charge goes backward than forward.

This result can be easily understood, at least qualitatively, in the following way: At small W vp scattering is dominated by a few exclusive final states, namely $p\pi^+$, $p\pi^+\pi^0$ (with $\langle Q \rangle_F \approx \langle Q \rangle_B \approx 1$) and $n\pi^+\pi^+$ with $\langle Q \rangle_F > \langle Q \rangle_B$ since the neutron goes mostly backward. These three channels thus lead to an overall excess of charge in forward direction. At high W on the other hand, the QPM predicts more charge going backward (from uu-

[2] Of course one always has $Q_F + Q_B = Q = 2$ for each event because of charge conservation.

-diquark) than going forward (from u-quark)[3]. This is also seen in Fig. 11c, which shows the distribution

$$\frac{d\langle Q\rangle}{dy} = \frac{1}{N_{ev}}\left(\frac{dN^+}{dy} - \frac{dN^-}{dy}\right) = \frac{d\langle n_+\rangle}{dy} - \frac{d\langle n_-\rangle}{dy} \tag{22}$$

of the average charge per event in cms rapidity y for two intervals of W. At high W there is more (positive) charge going backward than forward in the cm system. Furthermore,

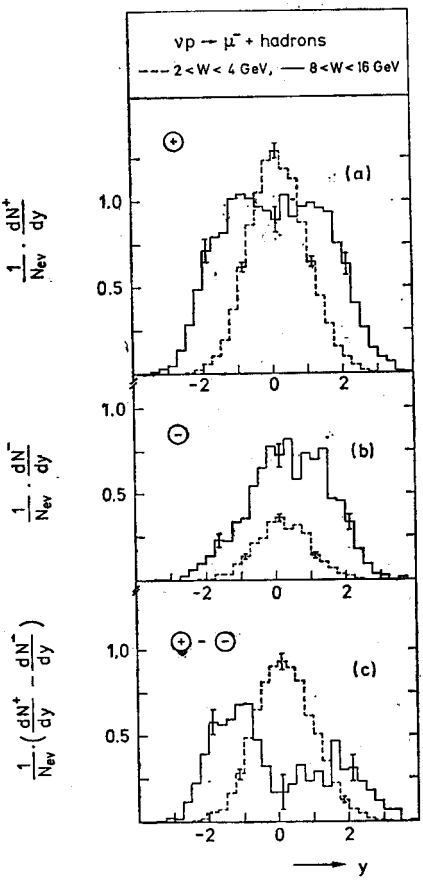

Fig. 11. cms rapidity distributions of (a) positive hadrons, (b) negative hadrons and (c) charge per νp event for two W intervals (dashed: $2 < W < 4$ GeV, full: $8 < W < 16$ GeV)

[3] However, already a simple model, in which the nucleon (~50% of the time a proton such that $\langle Q_N\rangle \approx \frac{1}{2}$) goes predominantly backward and the remaining charge is distributed at random gives a charge excess in the backward direction:

$$\langle Q\rangle_B = \tfrac{1}{2}+\tfrac{3}{4} = \tfrac{5}{4} \tag{21}$$
$$\langle Q\rangle_F = \tfrac{3}{4}$$

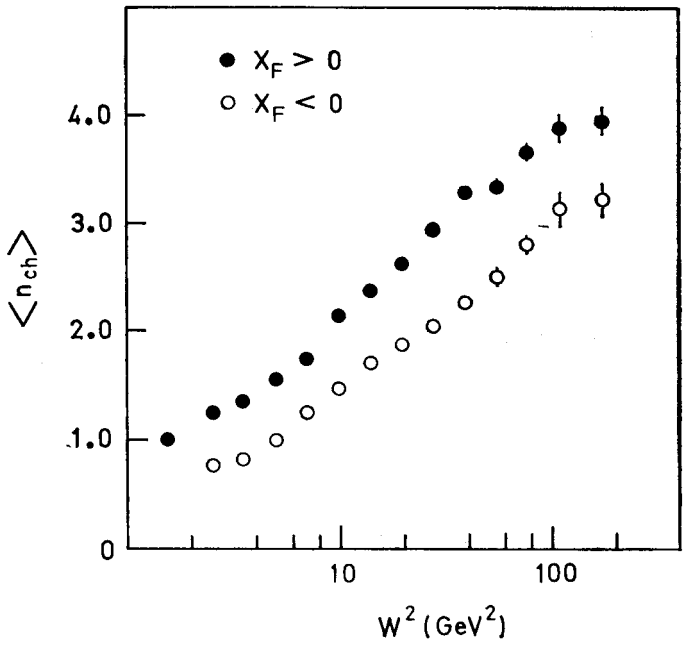

Fig. 12. Average multiplicity of charged hadrons going forward ($x_F > 0$) and backward ($x_F < 0$) in the hadronic cm system vs W^2 in νp scattering

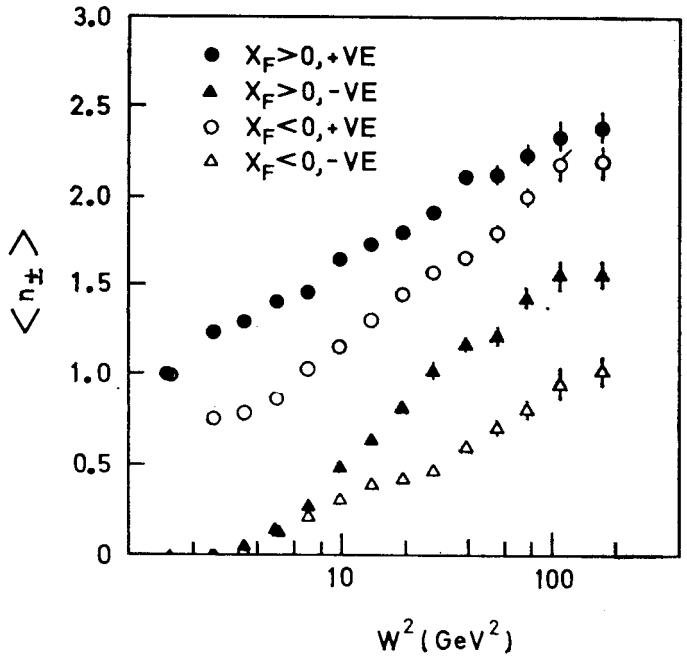

Fig. 13. Average multiplicity of positive and negative hadrons going forward ($x_F > 0$) and backward ($x_F < 0$) in the hadronic cm system vs W^2 in νp scattering

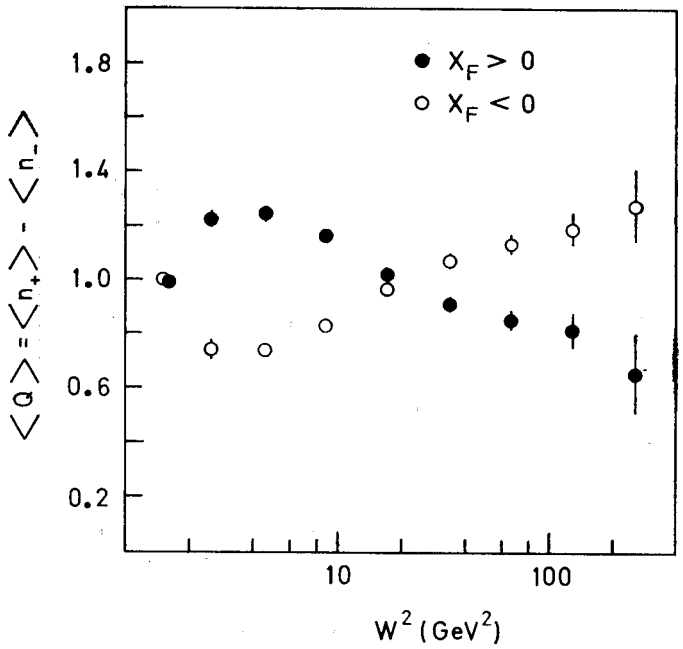

Fig. 14. Average charge per νp event going forward ($x_F > 0$) and backward ($x_F < 0$) in the hadronic cm system vs W^2. $Q_F + Q_B = 2$ for each event

for $W > 8$ GeV the charge distribution shows a clear step around $y = 0$, which is most likely due to a separation between current and target fragments. A similar step at $y \approx 0$ has been observed in the charge distribution for $\bar{\nu}$p scattering (where $Q = 0$) with $W > 4$ GeV by the Argonne, Carnegie-Mellon, Purdue Collaboration [22]. Thus it seems possible to separate (at least approximately) the target from the current fragments at high W by cutting at $y = 0$ (i.e. $x_F = 0$) in the cm system.

We now discuss the forward charge $\langle Q \rangle_F$ and its relation to the fragmentation of the u-quark in the QPM (Fig. 10) more quantitatively. Neglecting fragmentation into baryons, Field and Feynman [23] and others before [24] have shown, that in the QPM the average charge $\langle Q \rangle_q$ of hadrons (mesons) from the fragmentation of a quark q is related to the charge e_q of the quark q by

$$\langle Q \rangle_q = e_q - \sum_a \gamma_a e_a = e_q - e_{\langle q \rangle}. \tag{23}$$

Here γ_a is the probability for creating a quark-antiquark pair $a\bar{a}$ from the "sea"; the constant correction term $e_{\langle q \rangle} \equiv \sum_a \gamma_a e_a$, called the "charge-leakage term", is thus the charge of an "average" quark $\langle q \rangle$ created from the sea. Equation (23) is easily derived [12, 23, 24] from the rapidity diagram in Fig. 15 for the cascade model of quark fragmentation: Since in measuring $\langle Q \rangle_q$ one collects the charges of hadrons (mesons), the quark a of the last pair $a\bar{a}$ in the chain has to be excluded and its charge, occurring with weight γ_a, must be subtracted. The neutral $b\bar{b}$ pairs between q and $\bar{a}$ do not contribute to $\langle Q \rangle_q$.

It should be pointed out, that it is not possible to determine the quark charges e_q from a measurement of the average hadron charges $\langle Q\rangle_q$ since the leakage-term $e_{\langle q\rangle}$ in (23) is not known a priori. Only *differences*

$$\langle Q\rangle_q - \langle Q\rangle_{q'} = e_q - e_{q'} \tag{24}$$

of quark charges can be measured. In fact, neglecting the production of heavy mesons containing c quarks ($\gamma_c = 0$), i.e. using $\gamma_u + \gamma_d + \gamma_s = 1$, and making the minimum assump-

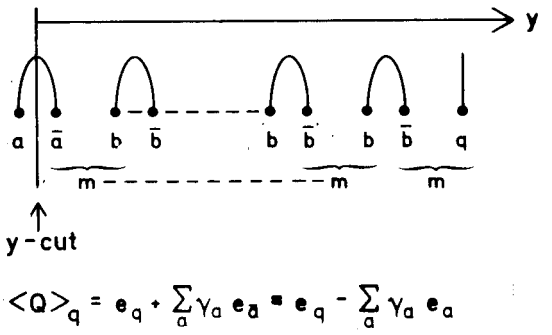

Fig. 15. Schematic rapidity diagram for the cascade model of quark fragmentation. The diagram shows how the average hadron charge $\langle Q\rangle_q$ is composed of the quark charges

tions $e_u - e_d = 1$ (π^+) and $e_u - e_s = 1$ (K^+) it follows from (23) that

$$\langle Q\rangle_u = 1-\gamma_u, \quad \langle Q\rangle_d = \langle Q\rangle_s = -\gamma_u$$
$$e_{\langle q\rangle} = e_u - 1 + \gamma_u. \tag{25}$$

Thus a measurement of the hadron charges $\langle Q\rangle_q$ yields the probability γ_u and not the quark charges. For SU(2) symmetry one has

$$\gamma_u = \gamma_d = \gamma, \quad \gamma_s = 1-2\gamma \tag{26}$$

and for an SU(3)-symmetric sea

$$\gamma_u = \gamma_d = \gamma_s = \gamma = \tfrac{1}{3}. \tag{27}$$

With the normal charge assignments to the quarks one obtains

$$e_{\langle q\rangle} = \gamma - \tfrac{1}{3} \; (= 0 \text{ for an SU(3)-symmetric sea}). \tag{28}$$

A clean measurement of $\langle Q\rangle_u$ in the present vp experiment can be obtained in the following way: Fig. 14 has shown that the average charge $\langle Q\rangle_F$ of forward going hadrons ($x_F > 0$) depends on W even at high W. This dependence is most likely due to an overlap between target and current fragments which still exists even at large (finite) W:

Current fragments are lost into the backward hemisphere and target fragments spill over into the forward hemisphere. Therefore, in order to achieve a clean separation of current and target fragments, an extrapolation of $\langle Q \rangle_F$ to infinite W should be carried out [25]. Fig. 16 shows the average forward charge $\langle Q \rangle_F$ per events vs $1/W$ together with a linear[4]

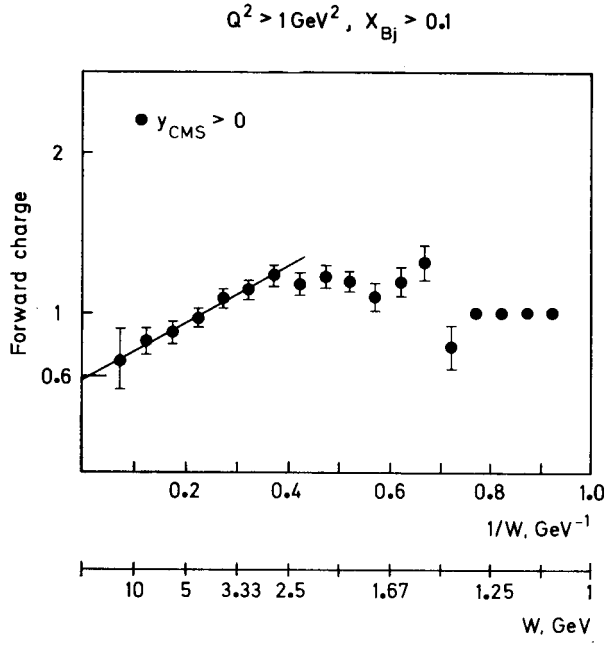

Fig. 16. Average forward charge per νp event vs $1/W$ for $x > 0.1$. The straight line shows a fit linear in $1/W$ to the first seven points ($W > 2.5$ GeV)

fit in $1/W$ to the first 7 data points ($W > 2.5$ GeV). The resulting extrapolated value at $1/W = 0$ is

$$\langle Q \rangle^{\nu}_{F,W=\infty} = \langle Q \rangle_u = 0.59 \pm 0.10$$

which yields according to Eq. (25):

$$\gamma_u = 0.41 \pm 0.10.$$

This value is in agreement with the result of the FIIM collaboration [25] which measured $\bar{\nu}$N interactions in the 15′ bubble chamber (so that the fragmenting quark is a d-quark) and obtained

$$\langle Q \rangle^{\bar{\nu}}_{F,W=\infty} = \langle Q \rangle_d = -0.44 \pm 0.09, \quad \gamma_u = 0.44 \pm 0.09 \quad \text{(see Eq. (25))}.$$

Finally, Fig. 17 shows the correlation parameter $f^{-}_{2F,B}$ vs $\langle n_- \rangle_{F,B}$ separately for the

[4] The linearity of the extrapolation in $1/W$ may be justified [25] by a correlation-length argument.

forward and backward hemispheres. In the backward hemisphere f_{2B}^{--} has a similar behaviour as f_2^{--} in pp scattering (see pp curve in Fig. 8). In the forward hemisphere f_{2F}^{--} is in good agreement with the prediction of the quark-fragmentation model of Field and Feynman [23].

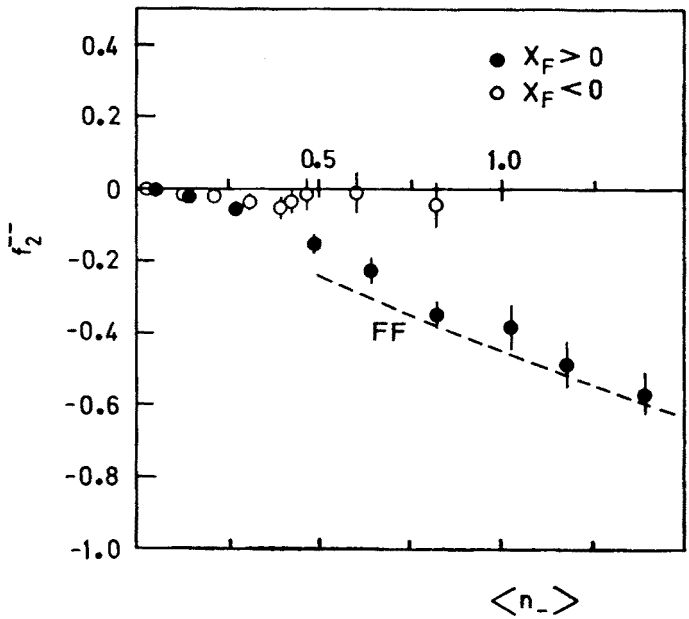

Fig. 17. Correlation parameter f_2^{--} vs average negative multiplicity in vp scattering separately for th-forward ($x_F > 0$) and backward ($x_F < 0$) cms hemispheres. The curve shows the prediction of the Field -Feynman cascade model [23] for quark fragmentation

C. Production of neutral strange particles, charm production

Starting from the four well-known charged weak quark currents the following eight transitions can occur in vp CC reactions:

(A) $d \to u$	(A′) $\bar{u} \to \bar{d}$	$\sim\cos^2\theta_c$	$\Delta Q = +1,\ \Delta S = \Delta C = 0$
(B) $s \to u$	(B′) $\bar{u} \to \bar{s}$	$\sim\sin^2\theta_c$	$\Delta Q = \Delta S = +1,\ \Delta C = 0$
(C) $d \to c$	(C′) $\bar{c} \to \bar{d}$	$\sim\sin^2\theta_c$	$\Delta S = 0,\ \Delta Q = \Delta C = +1$
(D) $s \to c$	(D′) $\bar{c} \to \bar{s}$	$\sim\cos^2\theta_c$	$\Delta Q = \Delta S = \Delta C = +1$

where the transitions A and C involve a valence quark and the others a sea quark in the nucleon. The processes C′, D′ are negligible because there is practically no $c\bar{c}$ sea in the nucleon. According to the above transitions the following sources exist for the production of strange particles in vp scattering:

Direct production:

— Process A (and A′) can lead to associated production of strange particles (ΛK^0, ΛK^+, $K\bar{K}$ etc.) via an $s\bar{s}$ pair occuring in the fragmentation of the u ($\bar{d}$) quark, see e.g. Fig. 18a.

— Processes B and B′ lead to the occurence of a single strange particle, which in B′ is a (forward going) strange particle containing the created $\bar{s}$ and in B a (backward going) strange particle containing the left-over $\bar{s}$ quark from the $s\bar{s}$ sea in the proton. However the contributions of these two processes are expected to be small because of the smallness of the sea and of the Cabibbo angle θ_c and can therefore be neglected.

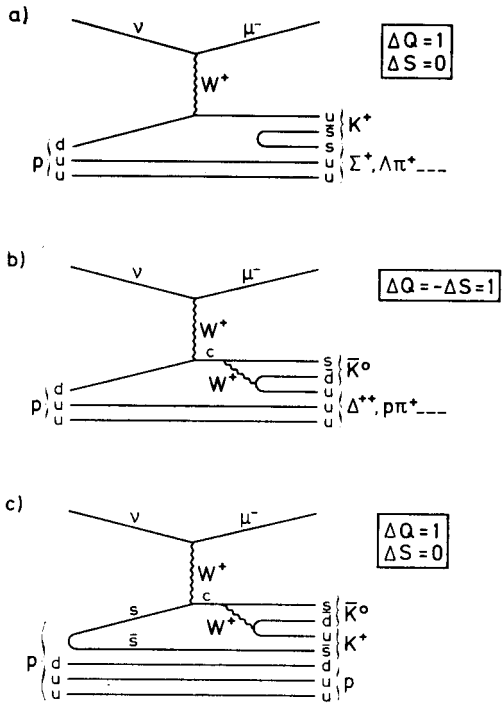

Fig. 18. Quark-diagrams contributing to strange particle production in νp scattering: (a) direct associated production, (b) charm production (on a valence d-quark) and decay leading to a single strange particle, (c) charm production (on a sea s-quark) and decay leading to two strange particles. (The final states are only examples)

Indirect production:

— via the decay of a c-quark, created in C or D, into an s-quark ($\sim\cos^2\theta_c$). In case C there is a single (forward going) strange particle (see e.g. Fig. 18b), whereas in case D there is in addition to this a (backward going) strange particle containing the left-over $\bar{s}$ quark from the $s\bar{s}$ sea (see e.g. Fig. 18c).

Thus, restricting oneself to the processes A, A′, C and D, one concludes that a single strange particle comes from the decay of a c-quark whereas strange particles occuring in pairs are either produced directly or in connection with the production and decay of a c-quark.

1. Rates of strange particle production

In the present experiment, 6770 CC events out of the total sample of ~7800 CC events had a W above the strange particle threshold, i.e. $W > 1.5$ GeV, and the subsequent analysis is carried out with these 6770 events only. The selected events had the following average values: $\langle E_\nu \rangle = 43$ GeV, $\langle Q^2 \rangle = 7$ GeV^2, $\langle W \rangle = 4.6$ GeV. Neutral strange particles (K_s^0, Λ, $\bar{\Lambda}$) in these events were identified by their characteristic decays and by mass fits to the measured decay tracks. (In case of a Λ/K^0 ambiguity the fit with the higher χ^2 probability was chosen.) A strange particle was accepted, if its path before decay was at least 1 cm and if the decay point was at least 10 cm away from the chamber wall. The resulting total numbers of observed strange particles are given in the upper part of Table I.

TABLE I

Observed and corrected numbers and corrected rates of strange particles and strange particle pairs

	Observed	Corrected	Rate [%]
K^0	359	1186	17.5±0.9
Λ	180	306	4.5±0.4
$\bar{\Lambda}$	13	22	0.3±0.1
K^0K^0	20	218	3.2±0.7
ΛK^0	18	103	1.5±0.4
$\Lambda\bar{\Lambda}$	4	11	0.2±0.1

The lower part of the table indicates how many of these strange particles were observed in pairs.

In order to obtain the true number of strange particles and strange-particle pairs, a weight was calculated in the usual manner for each accepted strange particle, which corrects for the minimal required decay path, the finite chamber size and the unobserved neutral decay modes (including the K_L^0 decay in case of a K^0). The resulting corrected numbers of strange particles and pairs are also given in Table I together with the production rates (= corrected numbers/number of CC events with $W > 1.5$ GeV).

We now give an estimate for the true number of *singly* produced Λ's, which according to the discussion above come from charmed baryon decay (process C). In order to obtain this number, one has to subtract from the total (corrected) number of Λ's the number of Λ's produced in association with an other strange particle, i.e. ΛK^0, ΛK^+, $\Lambda\bar{\Lambda}$. Only the number of ΛK^+ is unknown and an assumption has to be made for the cross section ratio

$$R = \frac{\sigma(\nu p \to \mu^- \Lambda K^+ + X)}{\sigma(\nu p \to \mu^- \Lambda K^0 + X)} . \tag{29}$$

In $\pi^+ p$ interactions at 16 GeV/c [26] the $\Lambda K^+/\Lambda K^0$ ratio has been measured to be $R = 1.4$, whereas at very high energies $R = 1$ is expected. Using the corrected numbers in Table I

one obtains a corrected number of 90 ± 46 (49 ± 54) single Λ's for $R = 1$ ($R = 1.4$), which corresponds to a production rate of $\sim 1.3\%$ ($\sim 0.7\%$). The errors on the particle numbers are unfortunately very large because of the small number of observed strange particle pairs. Similarly the true number of single K^0 ($\bar{K}^0$) can be estimated which originate from the production and subsequent decay of a charmed particle (process C). Assuming $\sigma(K^0K^0) = \sigma(K^0K^+) = \sigma(K^0K^-)$, $\sigma(K^0\Lambda) = 1.4\ \sigma(K^0\Sigma^\pm)$ [26] and using the corrected numbers in Table I, one obtains 138 ± 175 singly produced K^0's in the CC event sample, which corresponds to a production rate of $\sim 2.0\%$.

2. Differential cross sections

Figs. 19, 20, 21a give the corrected relative cross sections (= rates) for K^0 and Λ pro-

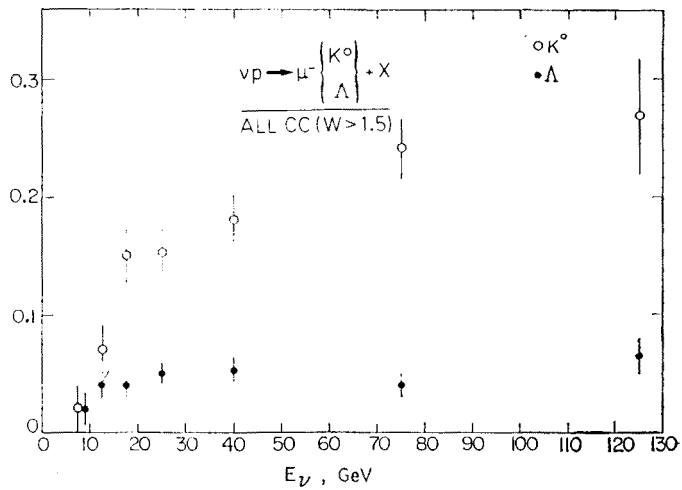

Fig. 19. Corrected relative cross sections for K^0 and Λ production in νp scattering vs neutrino energy E_ν

duction (i.e. corrected number of events containing at least one K^0 or Λ over number of CC events with $W > 1.5$ GeV) as functions of E_ν, Q^2 and W^2. It is seen that the Λ production rate is rather independent of E_ν, Q^2 and W^2 whereas the rate for K^0 production is a rising function of these variables. Fig. 21b, where the K^0 rate is plotted vs W^2 separately for forward and backward going K^0's, shows that the rise of the overall K^0 rate with W^2 is mainly due to the forward K^0's whereas the backward K^0's have an almost W^2 independent rate. This is expected if the forward K^0's come (partially) from the decay of charmed mesons which are produced mainly forward and have a production rate that rises with W^2.

In Fig. 22 the corrected rates for K^0 and Λ production are plotted vs Bjorken-x

$$x = \frac{Q^2}{2M\nu} \quad (\nu = E_\nu - E_\mu). \tag{30}$$

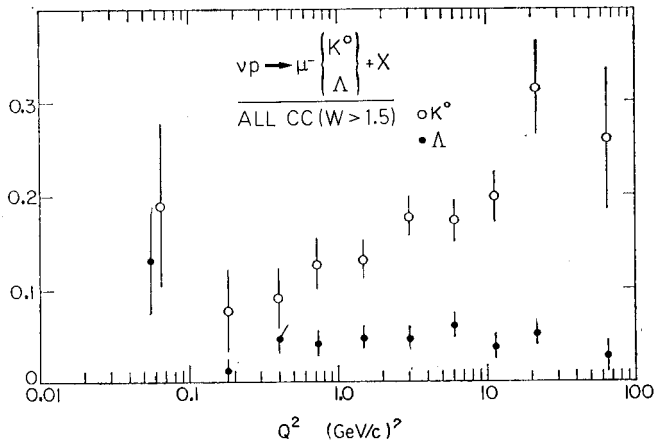

Fig. 20. Corrected relative cross sections for K^0 and Λ production in νp scattering vs Q^2

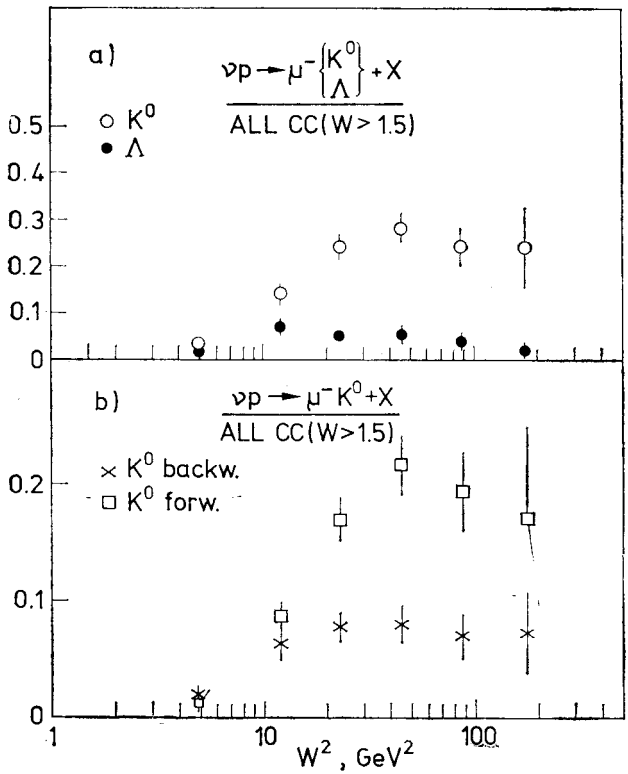

Fig. 21. Corrected relative cross sections (a) for K^0 and Λ production, (b) for K^0 production in the forward and backward cms hemispheres in νp scattering vs W^2

Both rates decrease with x. This indicates that sea quarks (which have a small x in the nucleon), i.e. process D (Fig. 18c), contribute appreciably to strange particle production. More quantitatively, Geich-Gimbel [27] has calculated the prediction of the QPM for the K^0 production rate in the following way: The two differential cross sections $\frac{d\sigma}{dx}(\nu p \to \mu^- + X)$ and $\frac{d\sigma}{dx}(\nu p \to \mu^- K^0 + X)$ can be expressed in terms of the x distribution functions of the contributing quarks in the usual manner. Knowing these distribution functions

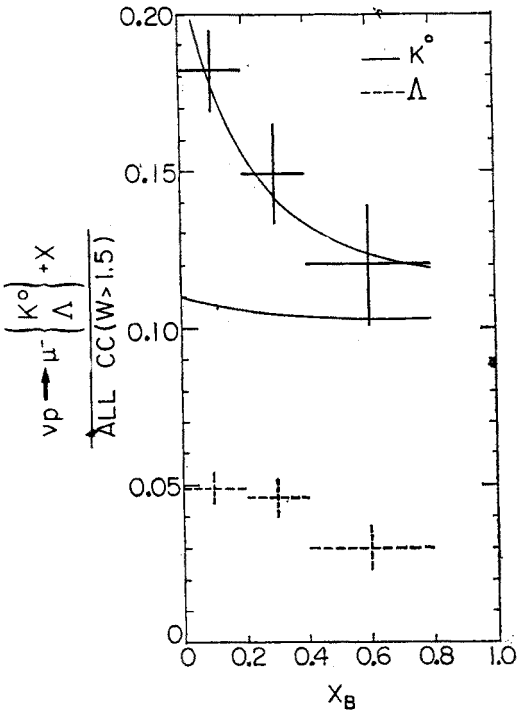

Fig. 22. Corrected relative cross sections for K^0 and Λ production in νp scattering vs Bjorken-x. The curves show the predictions of the quark-parton model: upper curve with charm production, lower curve without charm production

from other neutrino experiments, the ratio of the two cross sections, i.e. the K^0 rate can then be calculated as a function of x. The resulting predictions are shown by the two curves in Fig. 22, (a) including the processes, which lead to a c-quark (upper curve) and (b) without these processes (lower curve). Obviously agreement with the data is obtained only, if charm production (processes C, D) is included. The total charm production rate turns out to be $\sim 10\%$ in good agreement with the values obtained from the dilepton rates as measured in other neutrino experiments [28].

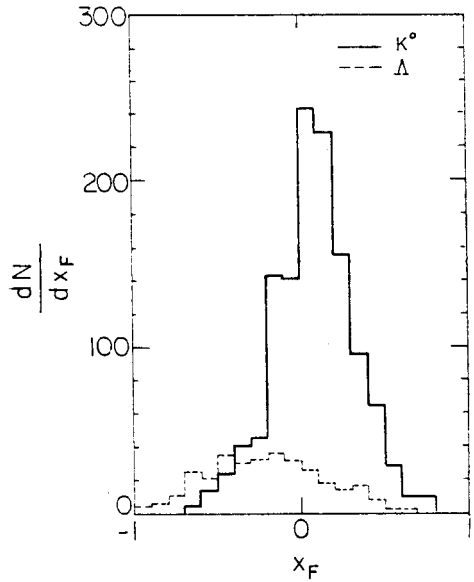

Fig. 23. Corrected Feynman-x_F distribution of K^0 and Λ produced in νp scattering.

From Fig. 23, which shows the corrected Feynman-x_F distributions for K^0 and Λ, it is seen that K^0's are produced predominantly forward, whereas most Λ's go backward in the hadronic cm system.

3. Fragmentation into K^0

Results on the effective fragmentation function

$$D_q^{K^0}(z) = \frac{1}{N_{ev}} \frac{dN_{K^0}}{dz} \tag{31}$$

are shown in Fig. 24. The index q stands for an average quark, since $D_q^{K^0}$ is a weighted sum of fragmentation functions of the various quarks contributing K^0's in the final state. The energy fraction z is here defined as $z = E_{K^0}/E_H$ where E_{K^0} and E_H are the K^0 energy and total hadronic energy, respectively, in the lab system. z distributions of the K^0 have also been measured in νN scattering with $\langle W \rangle = 3.3$ GeV [28], i.e. basically below the charm threshold, and in ep scattering with $\langle W \rangle = 3.15$ GeV [29], where charm production does not occur. However these distributions cannot be compared directly with Fig. 24, since the definitions of z are different in all three experiments.

Fig. 25 shows the z dependence of the following particle ratios: π^-/π^+, K^0/π^+, K^0/π^-. The π^-/π^+ ratio drops continuously as z increases whereas the K^0/π ratios first rise to reach a maximum around $z \approx 0.4$ and then drop off. Both behaviours can be understood in the cascade model for quark fragmentation [23]: The π^+ can contain the fragmenting u-quark from the main process A, $d \to u$, and is thus favoured to be the leading ("rank one" [23]) particle with high z, whereas the π^- is created later in the fragmentation chain (i.e. from

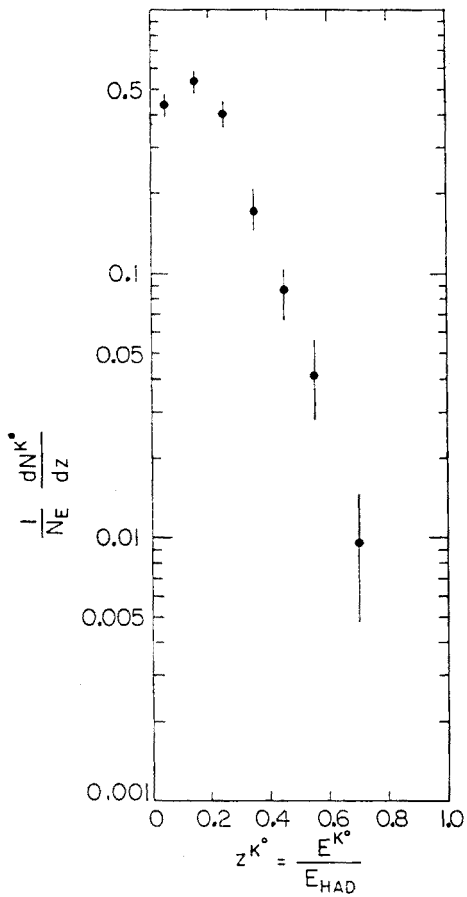

Fig. 24. Distribution of the hadronic energy fraction z, which is carried by K^0's per νp event

the sea) and thus has smaller z. The K^0 is expected predominantly at intermediate values of z, since in direct associated production (process A) it is produced from the sea (smaller z) whereas in production via decay of a charmed quark or meson (processes C, D) it is close to the c-quark in the cascading chain (higher z).

4. Resonance production

The $K_s^0\pi^+$ mass distribution in Fig. 26 shows a clear signal of $\sim 35 \pm 7$ observed $K^{*+}(890)$ events above a smooth handdrawn background. Applying the various corrections and taking into account the $K^+\pi^0$ decay mode this yields a rate of

$$\frac{\sigma(\nu p \to \mu^- K^{*+}_{890} + X)}{\sigma(\nu p \to \mu^- + X)} = (2.5 \pm 0.5)\%.$$

No signal has been observed either in the $K^0\pi^+$ or in the $K^0\pi^+\pi^-$ mass distribution in the mass region of the D mesons. A more careful analysis relying also on decay channels

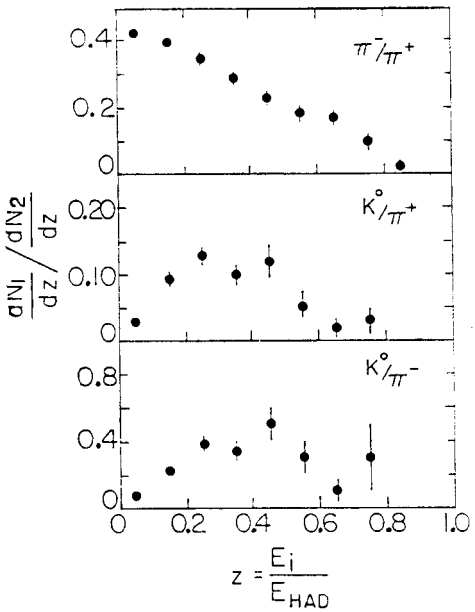

Fig. 25. Particle ratios (a) π^-/π^+, (b) K^0/π^+ and (c) K^0/π^- vs energy fraction z

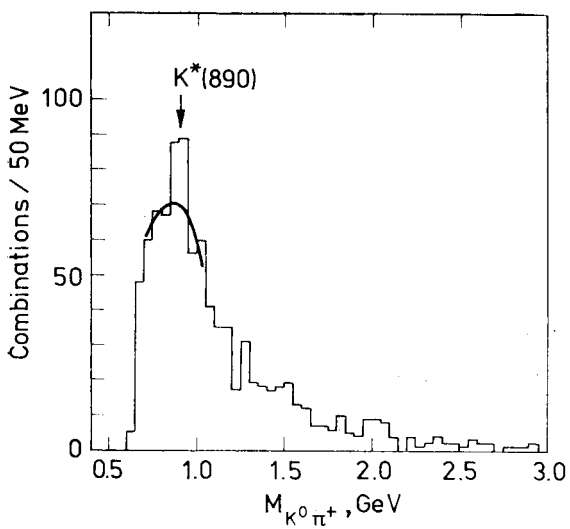

Fig. 26. $K^0_s\pi^+$ mass distribution in νp scattering

containing a K^- and exploiting the high measuring accuracy of the D*-D mass difference has yielded [4]

$$\frac{\sigma(\nu p \to \mu^- D^{*+} + X)}{\sigma(\nu p \to \mu^- + X)} = (4.1 \pm 2.4)\%.$$

In the $\Lambda\pi^+$ mass distribution, shown in Fig. 27, a clear signal of the $\Sigma^+(1385)$ is seen

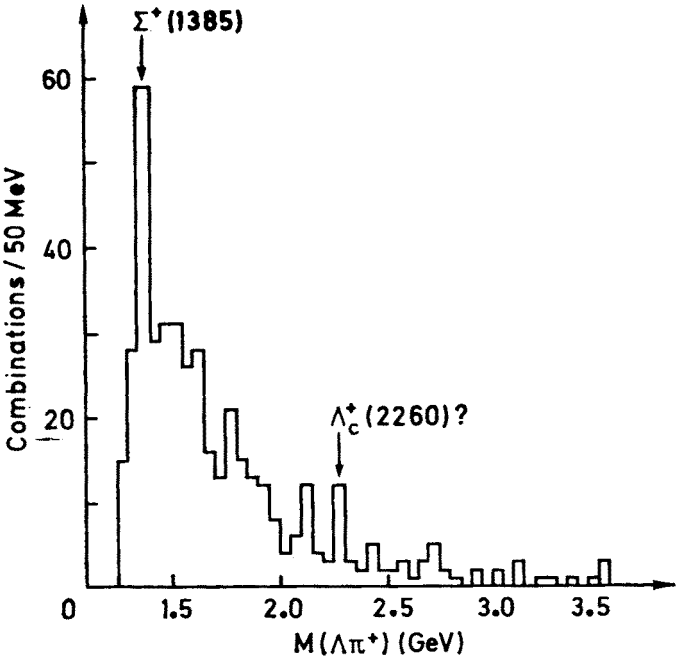

Fig. 27. $\Lambda\pi^+$ mass distribution in νp scattering

with 31 ± 6 events above background. This yields (after corrections and taking into account the $\Sigma\pi$ decay mode) a rate of

$$\frac{\sigma(\nu p \to \mu^- \Sigma^+_{1385} + X)}{\sigma(\nu p \to \mu^- + X)} = (0.9 \pm 0.2)\%.$$

No clear Λ_c^+ signal is observed neither in the $\Lambda\pi^+$ nor in the $\Lambda\pi^+\pi^+\pi^-$ mass distribution. If the 8 ± 3 events above background in the mass interval 2.25—2.30 GeV of the $\Lambda\pi^+$ mass distribution are due to $\Lambda_c^+(2.26)$ production then a rate of

$$\frac{\sigma(\nu p \to \mu^- \Lambda_c^+ + X) \quad \big| \to \Lambda\pi^+}{\sigma(\nu p \to \mu^- + X)} = (1.8 \pm 0.7) \cdot 10^{-3}$$

is obtained.

D. Moments of quark-singlet and gluon fragmentation functions

In previous publications [5, 10, 12] the fragmentation functions $D_u^{\pm}(z, Q^2)$ of the u-quark into positive and negative hadrons and their moments

$$D_u^{\pm}(m, Q^2) = \int_0^1 dz z^{m-1} D_u^{\pm}(z, Q^2) \tag{32}$$

were investigated and a scaling-violating Q^2 dependence was observed if no cut in W was applied. For the non-singlet (NS) fragmentation function $D_{NS}(z, Q^2)$ this Q^2 dependence was found to be in surprising agreement with the prediction [30] of leading-order QCD:

$$D_{NS}(m, Q^2) = C_m \left(\ln \frac{Q^2}{\Lambda^2} \right)^{-d_m^{NS}}, \tag{33}$$

where

$$d_m^{NS} = \frac{4}{33-2f} \left[1 - \frac{2}{m(m+1)} + 4 \sum_2^m \frac{1}{\mu} \right] \tag{34}$$

is the NS anomalous dimension and Λ the scale parameter occuring in the running coupling constant $\alpha(Q^2)$ of QCD:

$$\alpha(Q^2) = \frac{12\pi}{33-2f} \Big/ \ln \frac{Q^2}{\Lambda^2}. \tag{35}$$

f is the number of active flavors ($f = 3$ is used here). For Λ a value of $\Lambda = 0.54 \pm 0.08$ GeV was obtained. In this chapter we present experimental data on the moments $D_S(m, Q^2)$ of the quark-singlet (S) fragmentation function and investigate the question if their Q^2 dependence is also described by QCD. Preliminary results have been presented in Ref. [10, 12].

The singlet and non-singlet fragmentation functions D_S^h and D_{NS}^h into hadrons of type h can be expressed in terms of the measurable fragmentation functions $D_u^{\pm}$ in the following way: The singlet is defined as ($f = 3$)

$$D_S^h = \frac{1}{2f} (D_u^h + D_{\bar{u}}^h + D_d^h + D_{\bar{d}}^h + D_s^h + D_{\bar{s}}^h) \tag{36}$$

such that D_S^h is the fragmentation function of an "average" quark into h[5]. Assuming charge conjugation invariance ($D_q^h = D_{\bar{q}}^h$) and the secondary hadrons to be pions such that isospin symmetry (e.g. $D_u^{\pi^+} = D_d^{\pi^-}$) can be applied, one obtains for an SU(3)-symmetric sea:

$$\begin{aligned} D_{\bar{u}}^+ &= D_d^+ = D_s^+ = D_{\bar{s}}^+ = D_u^-, \\ D_{\bar{d}}^+ &= D_u^+. \end{aligned} \tag{37}$$

[5] We prefer the definition (36) instead of the usual one without the factor $1/2f$, since our definition has the simple meaning of an average fragmentation function and since with this definition the factor $2f$ does not occur in some of the subsequent formulae.

Therefore (for $h = \pi^+$ and $f = 3$):

$$D_S^+ = \tfrac{1}{3}(D_u^+ + 2D_u^-). \tag{38a}$$

By charge conjugation invariance

$$D_{NS}^+ = D_u^+ - D_{\bar{u}}^+ = D_u^+ - D_u^- \tag{38b}$$

is a non-singlet, irrespective of the nature of the hadron ($\pi^\pm$, $K^\pm$, $p/\bar{p}$). Thus the fragmentation functions D_S^+, D_{NS}^+ and their moments can be determined (under the assumptions made) from $D_u^\pm$ using Eq. (38).

The corrections of first-order QCD to the singlet and gluon fragmentation functions D_S^h and D_G^h are given by the Altarelli-Parisi integro-differential equations [31] for fragmentation functions [30]:

$$\frac{d}{dt} D_S^h(z,t) = \frac{\alpha(t)}{2\pi} \int_z^1 \frac{dy}{y} \left[P_{qq}\left(\frac{z}{y}\right) \cdot D_S^h(y,t) + P_{Gq}\left(\frac{z}{y}\right) \cdot D_G^h(y,t) \right] \tag{39a}$$

$$\frac{d}{dt} D_G^h(z,t) = \frac{\alpha(t)}{2\pi} \int_z^1 \frac{dy}{y} \left[2fP_{qG}\left(\frac{z}{y}\right) \cdot D_S^h(y,t) + P_{GG}\left(\frac{z}{y}\right) \cdot D_G^h(y,t) \right] \tag{39b}$$

with

$$t = \ln \frac{Q^2}{Q_0^2}, \quad \alpha \ln \frac{Q_0^2}{\Lambda^2} = \frac{12\pi}{33-2f} \quad (\alpha \equiv \alpha(t=0)).$$

D_G^h is the fragmentation function of the gluon. $P_{ba}(z)$ is the probability density to create by a QCD process a parton b from a parton a such that b carries a fraction z of the momentum of a. The QCD processes corresponding to the four terms of the integrands in Eq. (39) are sketched in Fig. 28. For the NS fragmentation function D_{NS}^h the gluon term

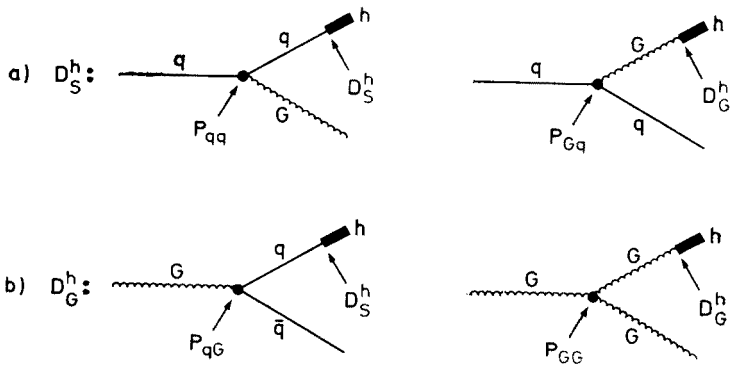

Fig. 28. First-order QCD processes leading to a Q^2-dependence of the quark-singlet (a) and gluon (b) fragmentation functions; see terms in Altarelli-Parisi equations (39)

in (39a) drops out such that

$$\frac{d}{dt} D^h_{\mathrm{NS}}(z, t) = \frac{\alpha(t)}{2\pi} \int_z^1 \frac{dy}{y} P_{qq}\left(\frac{z}{y}\right) \cdot D^h_{\mathrm{NS}}(y, t). \tag{39c}$$

The Altarelli-Parisi equations (39) are easily solved in terms of moments, defined in analogy to (32), with the result [30]:

$$D^h_{\mathrm{NS}}(m, Q^2) = D^h_{\mathrm{NS}}(m, Q_0^2) \cdot a_m^{\mathrm{NS}} \quad \text{(compare (33))} \tag{40a}$$

$$D^h_{\mathrm{S}}(m, Q^2) = D^h_{\mathrm{S}}(m, Q_0^2) \cdot [a_m^+ + A_m(a_m^- - a_m^+)] + D^h_{\mathrm{G}}(m, Q_0^2) \cdot C_m[a_m^+ - a_m^-] \tag{40b}$$

$$D^h_{\mathrm{G}}(m, Q^2) = D^h_{\mathrm{S}}(m, Q_0^2) \cdot \frac{A_m(1-A_m)}{C_m} [a_m^+ - a_m^-] + D^h_{\mathrm{G}}(m, Q_0^2) \cdot [a_m^- + A_m(a_m^+ - a_m^-)] \tag{40c}$$

with

$$a_m^i \equiv a_m^i(Q^2, Q_0^2) = \left(\ln \frac{Q_0^2}{\Lambda^2} \Big/ \ln \frac{Q^2}{\Lambda^2}\right)^{d_m^i} \qquad (i = \mathrm{NS}, +, -)$$

$$A_m = \frac{d_m^+ - d_m^{\mathrm{NS}}}{d_m^+ - d_m^-}, \qquad C_m = \frac{d_m^{\mathrm{G}q}}{d_m^+ - d_m^-}.$$

The d_m^i are the anomalous dimensions ($\propto$ moments of the probabilities $P_{ba}(z)$) in the notation of Ref. [32]. The parameters $D^h_{\mathrm{NS}}(m, Q_0^2)$, $D^h_{\mathrm{S}}(m, Q_0^2)$ and $D^h_{\mathrm{G}}(m, Q_0^2)$ are the NS, S and gluon moments to be determined from experiment at some normalisation point $Q^2 = Q_0^2$.

Introducing the ratios

$$R(m, Q^2) = \frac{D_{\mathrm{S}}^+(m, Q^2)}{D_{\mathrm{NS}}^+(m, Q^2)} \tag{41}$$

and

$$P(m, Q^2) = \frac{D_{\mathrm{G}}^+(m, Q^2)}{D_{\mathrm{S}}^+(m, Q^2)} \tag{42}$$

one obtains from (40a) and (40b):

$$\frac{R(m, Q^2)}{R(m, Q_0^2)} = B_1(m, Q^2, Q_0^2) + B_2(m, Q^2, Q_0^2) \cdot P(m, Q_0^2), \tag{43}$$

where

$$B_1(m, Q^2, Q_0^2) = \frac{a_m^+ + A_m(a_m^- - a_m^+)}{a_m^{\mathrm{NS}}} \quad \text{and} \quad B_2(m, Q^2, Q_0^2) = \frac{C_m(a_m^+ - a_m^-)}{a_m^{\mathrm{NS}}} \tag{44}$$

follow from theory. Thus, the QCD formula (43) can be fitted to the measured points

$$R(m, Q^2) = \tfrac{1}{3} \frac{D_{\mathrm{u}}^+(m, Q^2) + 2D_{\mathrm{u}}^-(m, Q^2)}{D_{\mathrm{u}}^+(m, Q^2) - D_{\mathrm{u}}^-(m, Q^2)} \tag{45}$$

with $R(m, Q_0^2)$ and $P(m, Q_0^2)$ as adjustable parameters.

For the present analysis the values $\Lambda^2 = 0.3\ \mathrm{GeV}^2$ and $Q_0^2 = 10\ \mathrm{GeV}^2$ have been chosen. Experimentally the fragmentation functions are given by

$$D_u^{\pm}(z, Q^2) = \frac{1}{N_{ev}(Q^2)} \frac{dN^{\pm}}{dz}(z, Q^2) \tag{46}$$

where $N_{ev}(Q^2)$ it the number of events at Q^2 and $N^{\pm}$ the number of positive and negative hadrons which are selected as current fragments in these events. z is the energy fraction carried by the hadron. Two different selection methods were adopted to separate (at least approximately) the current fragments from the target fragments:

1. Selection in the hadronic cm system

A hadron is taken as a current fragment if it goes forward ($x_F > 0$) in the hadronic cm system. In this case the energy fraction z is defined as[6]

$$z = \frac{\boldsymbol{p} \cdot \boldsymbol{h}}{\boldsymbol{p} \cdot \boldsymbol{q} + \boldsymbol{p}^2} = \frac{E_h}{E_H} = \frac{E_h}{\nu + M}, \tag{47}$$

where $\boldsymbol{p}$, $\boldsymbol{q}$, $\boldsymbol{h}$ are the four-momenta of the incident proton, the current (W^+) and the final state hadron respectively. E_h and E_H are the lab energy of the hadron and of all outgoing hadrons respectively.

2. Selection in the Breit system

A hadron is taken as a current fragment if it goes forward in the Breit frame[7]. In this case the energy fraction z is defined as

$$z_B = -\frac{2\boldsymbol{h} \cdot \boldsymbol{q}}{Q^2} = \frac{2p_{\parallel}^B}{Q}, \tag{48}$$

where $p_{\parallel}^B$ is the longitudinal momentum of the hadron in the Breit system. Thus $z_B > 0$ for current fragments.

We present the results for both selections although selection 1) is preferred over 2) as explained in section B (Fig. 11c), see also Ref. [12]. The experimental values for $R(m, Q^2)$ vs Q^2 are shown for $m = 2, 3, 5$ by the data points in Figs. 29 and 30 for the cms and Breit-frame selection respectively, (a) for the case that the identified protons are included in

---

[6] With this definition one always has $z \leqslant 1$ whereas the usually used $z = \frac{E_h}{\nu}$ may exceed one.

[7] The Breit system is the system, in which the W^+ has zero energy, i.e. momentum $Q = \sqrt{Q^2}$ and the current quark has momentum $\frac{Q}{2}$. The Breit system has the velocity $1 - 2x$ in the cm system, i.e. it goes forward (backward) in the cm system with respect to the current direction for $x < 0.5$ ($x > 0.5$). Since for most events $x < 0.5$ more hadrons go forward in the cm system than in the Breit system.

the particle sample and (b) for the identified protons being removed. No cut in W is applied. One sees that for $Q^2 > 1$ GeV^2 it practically makes no difference if one leaves the identified protons in or takes them out[8]. Furthermore the differences between the two selections become smaller with increasing m and Q^2.

The curves in Figs. 29 and 30 show the fits of Eq. (43) to the experimental points for $Q^2 > 1$ GeV^2. It is seen that the QCD formula (43) describes the experimental points rather well with χ^2/NDF values of ~ 1. It turns out that with the values chosen for Λ^2 and $Q_0^2 B_1(m, Q^2, Q_0^2)$ is almost constant (≈ 1), whereas $B_2(m, Q^2, Q_0^2)$ rises with Q^2. Thus

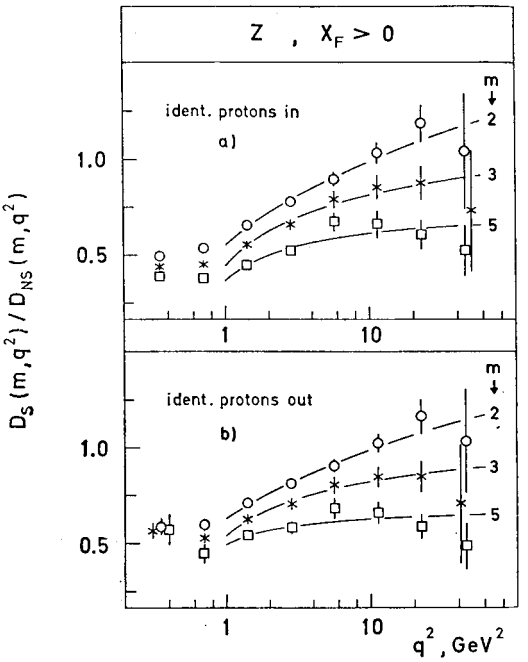

Fig. 29. Ratio $R(m, Q^2)$ of singlet-to-non-singlet fragmentation moments vs Q^2 for $m = 2, 3, 5$ for the cms selection; (a) identified protons included, (b) identified protons excluded. The curves are fits of the QCD formula (43) to the data points for $Q^2 > 1$ GeV^2

the observed rise of $R(m, Q^2)$ with Q^2 is due to the second term in Eq. (43), i.e. to gluon fragmentation.

The fitted values of $R(m, Q_0^2)$ and $P(m, Q_0^2)$ at $Q_0^2 = 10$ GeV^2 are shown in Fig. 31 as functions of m for the four cases (2 selections, identified protons in or out). The S to NS ratio $R(m, Q_0^2)$ does practically not depend on leaving the protons in or taking them out; it is systematically (i.e. for all m) larger for the cms than for the Breit-frame selection. For the $m = 2$ gluon-to-singlet ratio $P(m = 2, Q^2)$ one expects a value of ≈ 1 from the

[8] It turns out that by applying the cut $x_F > 0$ ($z_B > 0$) most of identified protons are removed anyway for $Q^2 > 1$ GeV^2.

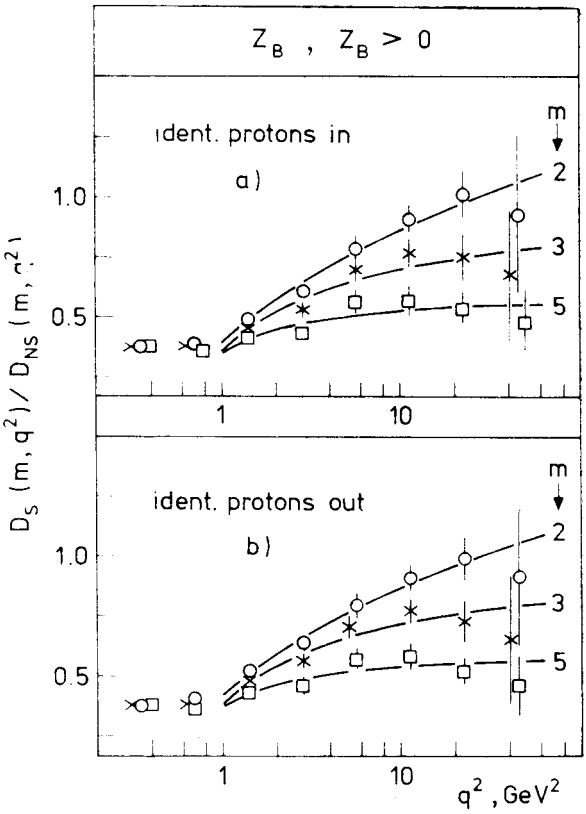

Fig. 30. Same as Fig. 29, but for the Breit-frame selection

energy conservation sum rules

$$\sum_h D_G^h(m = 2) = \sum_h \int_0^1 z D_G^h(z) dz = 1$$

$$\sum_h D_S^h(m = 2) = \sum_h \int_0^1 z D_S^h(z) dz = 1 \qquad (49)$$

if one assumes that in both cases the same energy fraction goes into charged hadrons (and using $D_{S,G}^+ = D_{S,G}^-$). It is seen from Fig. 31 that $P(m = 2, Q_0^2)$ is closer to one for the cms selection than for the Breit selection. For larger m the gluon moments seem to be larger than the singlet moments at $Q_0^2 = 10\,\text{GeV}^2$, the actually fitted value of the ratio $P(m, Q_0^2)$ depending on which selection is chosen and on leaving the identified protons in or taking them out.

Knowing the ratios $R(m, Q_0^2)$ and $P(m, Q_0^2)$ and normalising to $D_{NS}^+(m, Q_0^2) = 1$ at $Q_0^2 = 10\,\text{GeV}^2$, the NS, S and gluon moments are then predicted as functions of Q^2 by the QCD formulae (40). As an example Fig. 32 shows the predicted $m = 3$ and 5 moments vs. Q^2 for the cms selection with the identified protons taken out. The gluon moments have a steeper fall-off with Q^2 than the S and NS moments.

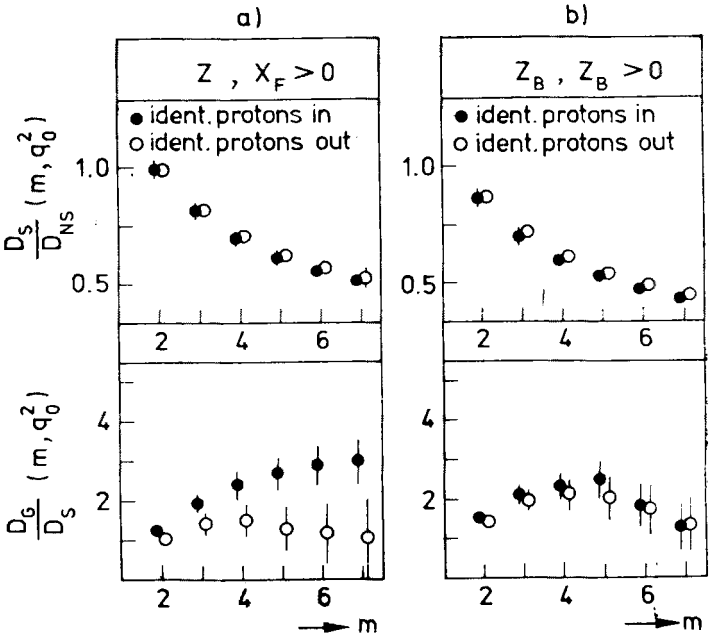

Fig. 31. Fitted values of the singlet-to-non-singlet ratio $R(m, Q_0^2)$ and of the gluon-to-singlet ratio $P(m, Q_0^2)$ at $Q_0^2 = 10\,\mathrm{GeV}^2$ vs m; (a) cms selection, (b) Breit-frame selection

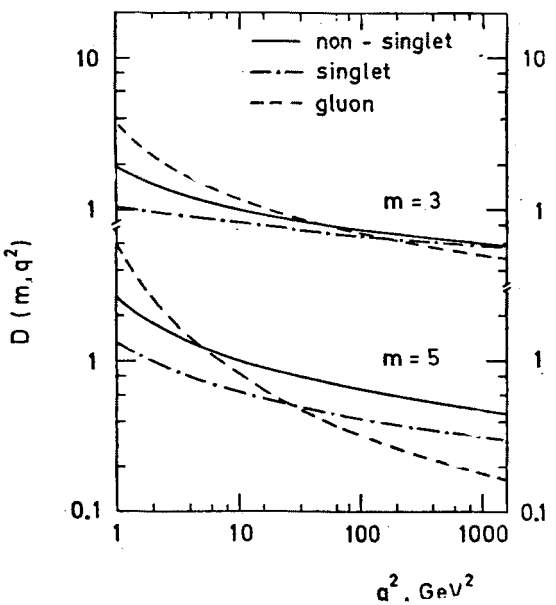

Fig. 32. Predicted non-singlet, singlet and gluon fragmentation moments for $m = 3$ and 5 vs Q^2. The parameters $R(m, Q_0^2)$ and $P(m, Q_0^2)$ have been taken from the fit with the cms selection and the identified protons being excluded. $D_{NS}(m, Q_0^2)$ was set to unity at $Q_0^2 = 10\,\mathrm{GeV}^2$

E. Non-factorisation and double moments

The semi-inclusive cross section for the production of a hadron h in the reaction

$$\nu p \to \mu^- h + X \tag{50}$$

in which (neglecting the sea in the nucleon) only one quark flavor is involved (see Fig. 10), may in general be written as

$$\frac{d\sigma^h}{dx dQ^2 dz}(x, Q^2, z) = \frac{d\sigma_{ev}}{dx dQ^2}(x, Q^2) \cdot D^h(x, z, Q^2) \tag{51}$$

where $\frac{d\sigma_{ev}}{dx dQ^2}$ is the inclusive event cross section in x (Eq. (30)) and Q^2 (Eq. (5)) for reaction (1) and $D^h(x, z, Q^2)$ a generalized fragmentation function. If h is a current fragment, lowest-order perturbative QCD predicts factorisation of the semi-inclusive cross section in x and z at fixed Q^2, i.e.

$$D^h(x, z, Q^2) = D^h(z, Q^2) \tag{52}$$

to be independent of x. In next-to-leading order of QCD a violation of factorisation is expected, as has been calculated by Sakai [33] and Altarelli et al. [34]. Experimentally, non-factorisation has been observed in previous publications [5, 12] of the present experiment; the moments of the fragmentation functions were found to depend on x at low Q^2, whereas for large $Q^2 > 10\,\mathrm{GeV}^2$ no significant x-dependence was observed.

A more quantitative way to study non-factorisation is an analysis in terms of double moments [33, 34]. They are defined as

$$D^h(n, m, Q^2) = \frac{\int_0^1 dx x^{n-1} \int_0^1 dz z^{m-1} \frac{d\sigma^h}{dx dQ^2 dz}}{\int_0^1 dx x^{n-1} \frac{d\sigma_{ev}}{dx dQ^2}} \tag{53}$$

and measured as

$$D^h(n, m, Q^2) = \frac{\sum_{i,j} x_i^{n-1} z_j^{m-1}}{\sum_i x_i^{n-1}}, \tag{54}$$

where the index i runs over all events at Q^2 and j over all current fragments of type h in these events. For $n = 1$ one obtains the previous formulae (32), (46) for the fragmentation moments. If factorisation holds, it follows from (51), (52) and (53), that the double moments become independent of n.

Experimental double moments were determined according to Eq. (54). Hadrons which go forward in the hadronic cms were selected as current fragments and the energy fraction z was calculated according to Eq. (47). Instead of x the Nachtmann variable

$$\xi = \frac{2x}{1+\sqrt{1+4M^2x^2/Q^2}} \tag{55}$$

was used in (54) for each event in order to account for target mass effects[9]. No cut in W was applied.

Since in the actual experiment the neutrino energy E_ν is finite and a cut $E_\mu > E_{\text{cut}} = 3$ GeV has been applied to the muon energy E_μ, the lower experimental limit of x at fixed Q^2 and E_ν is not zero as in Eq. (53), but

$$x_1 = \frac{Q^2}{2M(E_\nu - E_{\text{cut}})} \tag{56}$$

as follows directly from the definition of Bjorken-x, Eq. (30). Furthermore the events are weighted according to the energy spectrum $\phi(E_\nu)$ of the incident neutrinos (Fig. 1). For these two reasons the measured double moments (54) are related, as is easily derived, to he differential cross sections by

$$D^h(n, m, Q^2) = \frac{\int_{E_{\min}}^{E_{\max}} dE\phi(E) \int_{x_1}^{1} dx x^{n-1} \int_0^1 dz z^{m-1} \frac{d\sigma^h}{dxdQ^2dz}}{\int_{E_{\min}}^{E_{\max}} dE\phi(E) \int_{x_1}^{1} dx x^{n-1} \frac{d\sigma_{\text{ev}}}{dxdQ^2}}, \tag{57}$$

where $E_{\min} = \frac{Q^2}{2M} + E_{\text{cut}}$ and $E_{\max}$ is the minimum and maximum neutrino energy. Thus formula (57) takes into account the experimental conditions, under which the double moments are measured; it will therefore be used now to compute from the theoretical differential cross sections the predictions for the double moments, which will then be compared with the experimental results. We follow the theoretical work of Altarelli et al. [34] who have calculated the differential cross sections in next-to-leading order of perturbative QCD to obtain non-factorisation.

The inclusive event cross section is given by

$$\frac{d\sigma_{\text{ev}}}{dxdQ^2} = \frac{G^2}{2\pi}\left[\left(1-\frac{x_0}{x}\right)\tilde{F}_2(x) + \frac{x_0^2}{2x^2}\tilde{F}_1(x) - \frac{x_0}{x}\left(1-\frac{x_0}{2x}\right)\tilde{F}_3(x)\right] \tag{58}$$

with

$$x_0 = \frac{Q^2}{2ME_\nu},$$

[9] It turned out that using x or using ξ made practically no difference.

where the structure functions $\tilde{F}_i(x)$ are related to the usual structure functions $F_i(x)$ by $(\tilde{F}_1, \tilde{F}_2, \tilde{F}_3) = (2F_1, F_2/x, F_3)$. For νp scattering they are given in next-to-leading order of perturbative QCD by [34]

$$\tilde{F}_2(x) = 2[d(x)+\bar{u}(x)]$$

$$\tilde{F}_1(x) = 2\int_x^1 \frac{dy}{y}\left\{[d(y)+\bar{u}(y)]\left[\delta\left(1-\frac{x}{y}\right) - \frac{4\alpha}{3\pi}\frac{x}{y}\right] - 2G(y)\frac{\alpha}{\pi}\frac{x}{y}\left(1-\frac{x}{y}\right)\right\}$$

$$\tilde{F}_3(x) = 2\int_x^1 \frac{dy}{y}[-d(y)+\bar{u}(y)]\left[\delta\left(1-\frac{x}{y}\right) - \frac{2\alpha}{3\pi}\left(1+\frac{x}{y}\right)\right]. \tag{59}$$

Here $d(x)$, $\bar{u}(x)$, $G(x)$ are the distribution functions of the d-quark, $\bar{u}$-quark and gluon in the proton. The Q^2 dependence of the structure functions, distribution functions and of the running coupling constant α is not written here explicitly. It is seen from (59) that only for $\alpha = 0$ and $\bar{u} = 0$ $\tilde{F}_1 = \tilde{F}_2 = -\tilde{F}_3$. In this context it should be noted that the Callan-Gross relation $\tilde{F}_1 = \tilde{F}_2$ is violated in the same order of QCD in which non-factorisation is predicted.

Similarly the non-singlet semi-inclusive cross section is given by

$$\frac{d\sigma_{\mathrm{NS}}}{dxdQ^2dz} = \frac{d\sigma^+}{dxdQ^2dz} - \frac{d\sigma^-}{dxdQ^2dz}$$

$$= \frac{G^2}{2\pi}\left[\left(1-\frac{x_0}{x}\right)\tilde{F}_2(x,z) + \frac{x_0^2}{2x^2}\tilde{F}_1(x,z) - \frac{x_0}{x}\left(1-\frac{x_0}{2x}\right)\tilde{F}_3(x,z)\right] \tag{60}$$

with [34]

$$\tilde{F}_{1,2}(x,z) = 2\int_x^1 \frac{dy}{y}\int_z^1 \frac{dz'}{z'}\left\{[d(y)+\bar{u}(y)]\tilde{F}_{qq}^{1,2}\left(\frac{x}{y}, z'\right) + 2G(y)\tilde{F}_{qG}^{1,2}\left(\frac{x}{y}, z'\right)\right\} D_{\mathrm{u}}^{\mathrm{NS}}\left(\frac{z}{z'}\right)$$

$$\tilde{F}_3(x,z) = 2\int_x^1 \frac{dy}{y}\int_z^1 \frac{dz'}{z'}[-d(y)+\bar{u}(y)]\tilde{F}_{qq}^{3}\left(\frac{x}{y}, z'\right) D_{\mathrm{u}}^{\mathrm{NS}}\left(\frac{z}{z'}\right). \tag{61}$$

Here the relation $D_{\mathrm{u}}^{\pm} = D_{\mathrm{d}}^{\pm}$ has been used, which is justified, since most secondary hadrons are pions. Furthermore the gluon fragmentation function drops out in the non-singlet case since $D_{\mathrm{G}}^{+} = D_{\mathrm{G}}^{-}$. The Q^2 dependence of the various functions is again not written explicitly. The next-to-leading-order QCD formulae for the parton structure functions $\tilde{F}_{p_1p_2}^{i}(x,z)$ are given by Eqs. (58) to (61) of Ref. [34] and are not repeated here.

Formulae (58) to (61) have been inserted into (57) and the three integrations have been performed, over x and z analytically and over E numerically. For the three distribution functions $d(x, Q^2)$, $\bar{u}(x, Q^2)$ and $G(x, Q^2)$ the expressions of Buras and Gaemers [35] have been adopted which have (approximately) the Q^2 dependence as predicted by leading-

-order QCD. For the moments $D_u^{NS}(m, Q^2) = D_u^+(m, Q^2) - D_u^-(m, Q^2)$ of the NS fragmentation function the QCD expression (33) was applied with $\Lambda^2 = 0.3\ \mathrm{GeV}^2$ such that for a given m the only free parameter is C_m.

We now present the experimental results on double NS moments $D_{NS}(n, m, Q^2) = D^+(n, m, Q^2) - D^-(n, m, Q^2)$ and compare these results with the theoretical predictions. Preliminary results have been published in Ref. [5, 12] were several approximations were made (e.g. $\tilde{F}_1 = \tilde{F}_2 = -\tilde{F}_3$) and a different definition of the z variable and of the current fragments (Breit-frame selection) was used. In Fig. 33 the NS double moments $D_{NS}(n, m, Q^2)$

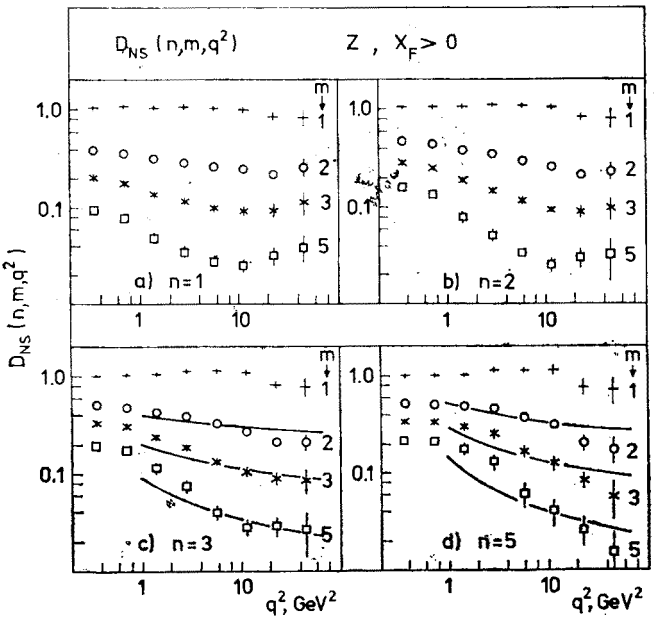

Fig. 33. Non-singlet double moments $D_{NS}(n, m, Q^2) = D^+(n, m, Q^2) - D^-(n, m, Q^2)$ vs Q^2 for $n = 1, 2, 3, 5$ and $m = 1, 2, 3, 5$. The curves are the predictions of next-to-leading order QCD normalized so that for $n = 5$ the curves coincide with the experimental points at $Q^2 \approx 10\ \mathrm{GeV}^2$

are plotted vs Q^2 for $n = 1, 2, 3, 5$ and $m = 1, 2, 3, 5$. For fixed m the moments depend on n in the region $1 \lesssim Q^2 \lesssim 10\ \mathrm{GeV}^2$ (non-factorisation). Above $Q^2 \simeq 10\ \mathrm{GeV}^2$ the moments are consistent with being independent of n at fixed m, i.e. with factorisation. The curves in Fig. 33 are the QCD predictions, Eq. (57) to (61), with the free parameters C_m determined so that for $n = 5$ the curves coincide with the experimental points at $Q^2 \approx 10\ \mathrm{GeV}^2$. The normalisation for $n \neq 5$ is then fixed by the theory. The QCD predictions are not shown for $n = 1, 2$ since for these moments the next-to-leading order QCD corrections turn out to be of similar size as the leading order contributions themselves and are thus unreliable. From Fig. 33 one sees that for $n = 3, 5$ and $m = 2, 3, 5$ the observed decrease of the double moments with Q^2 is stronger than predicted. On the other hand the increase with increasing n at fixed m in the region $1 \lesssim Q^2 \lesssim 10\ \mathrm{GeV}^2$ is qualitatively reproduced by the theory.

Non-factorisation may be seen more clearly in ratios of double moments [33]:

$$S_1(n_1, n_2, m) = \frac{D_{NS}(n_2, m)}{D_{NS}(n_1, m)}, \tag{62}$$

$$S_2(n_1, m_1; n_2, m_2) = \frac{D_{NS}(n_1, m_1) \cdot D_{NS}(n_2, m_2)}{D_{NS}(n_1, m_2) \cdot D_{NS}(n_2, m_1)}. \tag{63}$$

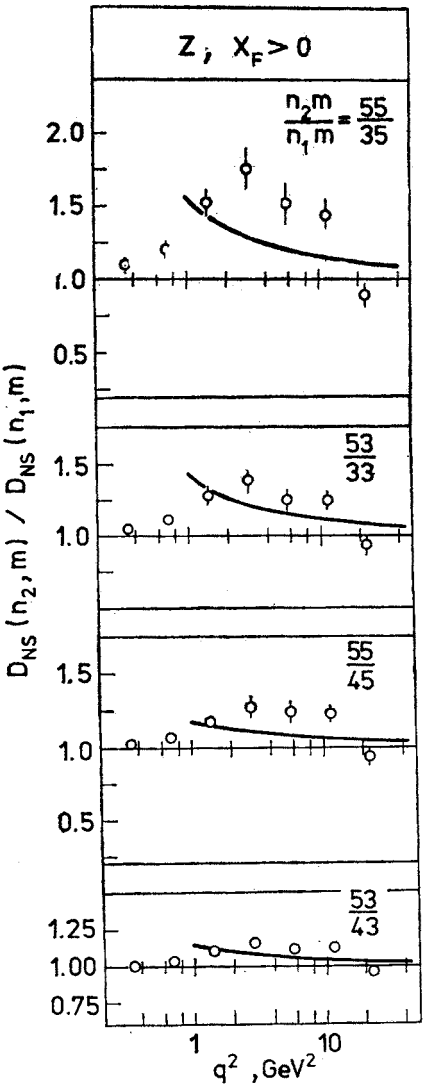

Fig. 34

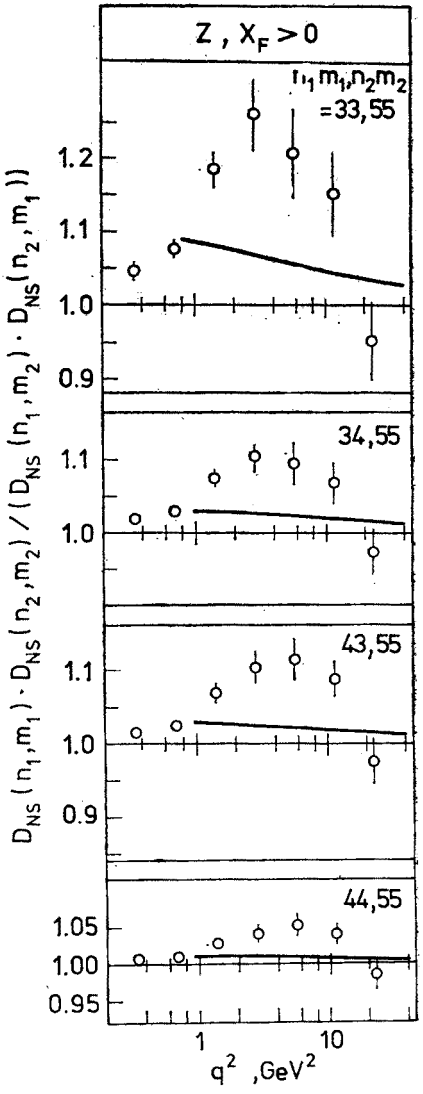

Fig. 35

Fig. 34. Ratios $S_1(n_1, n_2, m) = D_{NS}(n_2, m)/D_{NS}(n_1, m)$ (see Eq. (62)) vs Q^2. The curves are the predictions of next-to-leading order QCD

Fig. 35. Ratios $S_2(n_1, m_1; n_2, m_2)$ (see Eq. (63)) vs Q^2. The curves are the predictions of next-to-leading order QCD

Both ratios should be unity for factorisation and thus measure the deviation from factorisation. It is seen from (60) and (61) that the fragmentation moments $D_u^{NS}(m, Q^2)$ with the unknown constants C_m cancel in the theoretical expressions for S_1 and S_2 such that the QCD predictions become absolute. Figs. 34 and 35 show some of these ratios S_1 and S_2 respectively as functions of Q^2 together with the theoretical curves. The observed Q^2 dependence is similar for all plotted ratios, showing the strongest deviation from factorisation in the region $2 \lesssim Q^2 \lesssim 10\ \mathrm{GeV}^2$. Agreement with theory exists only in the sign of the deviation, but not in absolute magnitude.

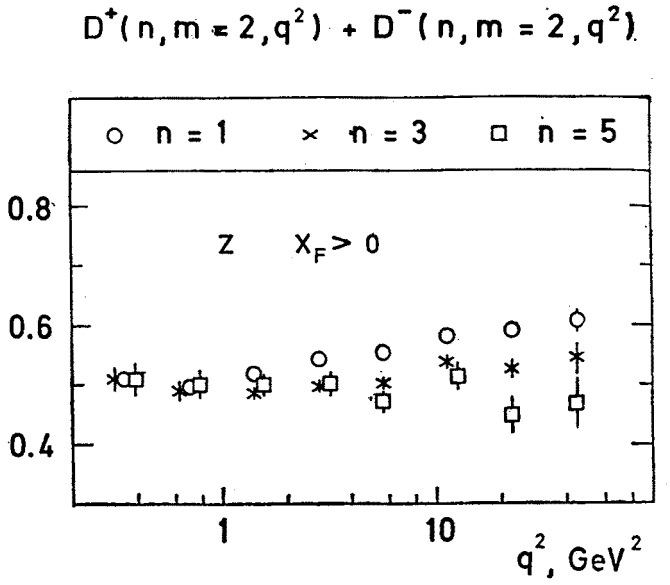

Fig. 36. Double moments $D^+(n, m = 2, Q^2) + D^-(n, m = 2, Q^2)$ vs Q^2 for $n = 1, 3, 5$

Finally, Fig. 36 shows the sum $D^+(n, m, Q^2) + D^-(n, m, Q^2)$ vs. Q^2 for $m = 2$ and various n. Because of the relation

$$D_u^+(m = 2) + D_u^-(m = 2) = \int_0^1 z[D_u^+(z) + D_u^-(z)]dz \tag{64}$$

this sum measures the fraction of the u-quark energy that is carried by the charged hadron fragments. Values between ~ 0.45 to ~ 0.6 are found for this energy fraction, systematically below a value of $\frac{2}{3}$ which is expected if an equal amount of energy goes into positive, negative and neutral fragments.

It should be mentioned that a scaling-violating Q^2 dependence of fragmentation functions and non-factorisation of the semi-inclusive cross section are also expected from higher twist effects. These effects are expected to become important at low Q^2 and large z. Quantitative predictions have been made by Berger [36] for the leptoproduction of pions. These predictions have not yet been applied to the data of this experiment.

F. Transverse momentum and jet studies

In this chapter the transverse momentum $\vec{p}_T$ of a secondary charged hadron is usually measured with respect to the direction $\hat{q}$ of the current, i.e. of the exchanged intermediate boson W^+ in reaction (3) $W^+p \to$ hadrons. This direction is known, once the energy of the incident neutrino is determined (see Introduction). As Fig. 37 shows, $\vec{p}_T$ can be decomposed

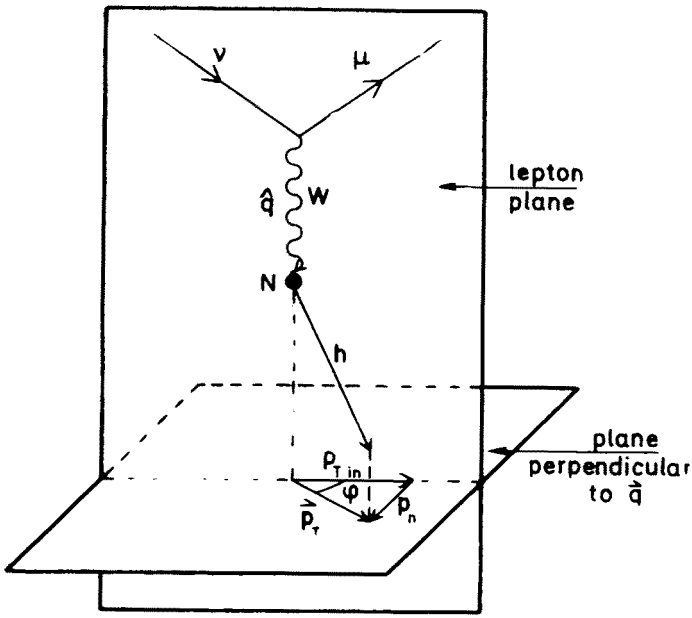

Fig. 37. Definition of the transverse momentum $\vec{p}_T$ of a secondary hadron with components p_{Tin} in, and p_n normal to the lepton plane

into components p_{Tin} in the lepton plane and p_n perpendicular to the lepton plane. The component p_n can be measured quite accurately, since the lepton plane is well defined. On the other hand, the current direction $\hat{q}$ in the lepton plane is not so well known due to the uncertainty in estimating the incident neutrino energy which leads to a less accurate measurement of the component p_{Tin}. For an isotropic distribution around the current direction one expects

$$\langle p_n^2 \rangle = \tfrac{1}{2} \langle p_T^2 \rangle. \tag{65}$$

As explained in chapter B, hadrons may be subdivided into those going forward (i.e. in $\hat{q}$ direction, $x_F > 0$) and backward (i.e. opposite to $\hat{q}$, $x_F < 0$) in the hadronic cm system (= W^+p cms) which in the simple QPM at high W (Fig. 10) corresponds to subdividing them into current and target fragments respectively.

The following sources, sketched in Fig. 38, are responsible for the transverse momenta of secondary hadrons:

— The simple QPM (zeroth-order QCD, Fig. 38a) yields a parton-final state with a forward going current quark and a backward going diquark, back-to-back to each other and

both with $p_T = 0$. Both then fragment into hadrons which in this non-perturbative hadronisation process acquire transverse momenta p_T^{frag}. The hadronic final state thus consists of two hadronic jets which both have a total transverse momentum of zero.

— In first-order QCD, there are three hard QCD processes in addition, which occur predominantly under not too large angles. All three result in a final state of three hadronic jets which may be separable from each other only at very high W:

● A hard gluon may be radiated off the current quark *after* the absorption of the current (Fig. 38b). The p_T distribution of the forward hadrons (from current-quark and gluon fragmentation) is expected to become wider whereas that of the backward hadrons (from diquark fragmentation) remains unchanged as compared to Fig. 38a. The widening in forward direction should increase with the hadronic cms energy W (as has been directly observed in e^+e^- annihilation at PETRA) since hard-gluon emission should become more and more noticeable. Eventually at very high W it should be possible to subdivide the forward hadrons into two separate jets.

● A hard gluon may be radiated off the current quark *before* the absorption of the current (Fig. 38c). As is seen intuitively from the figure, this may lead to a widening of the p_T distributions both in the forward and backward hemisphere[10].

● A gluon in the incoming nucleon may convert into a $q\bar{q}$ pair before one of the two quarks absorbs the current (Fig. 38d). Similar to the previous process this may lead to a widening of the p_T distributions both in the forward and backward hemisphere[10]. All three QCD processes lead to a transverse momentum k_T^{QCD} of the forward going partons.

— Finally the partons in the nucleon may have a primordial transverse momentum k_T^{prim} (Fig. 38e). Without QCD, the parton-final state consists of a current quark and a diquark, back-to-back to each other and with a transverse momentum k_T^{prim}. After hadronisation the hadronic final state consists of two hadronic jets and the hadronic p_T distributions with respect to $\hat{q}$ are widened as compared to Fig. 38a in both hemispheres. There may of course be hard QCD effects in addition.

The average p_T^2 of a forward-going hadron is thus composed of the contributions discussed, namely primordial transverse momentum, hard QCD processes and non-perturbative fragmentation in the following way:

$$\langle p_T^2 \rangle_F = [\langle k_T^{2prim} \rangle + \langle k_T^{2QCD} \rangle] \langle z^2 \rangle + \langle p_T^{2frag} \rangle \tag{66}$$

[10] Quantitatively however, the widening of the p_T distribution for hadrons in the backward direction, in particular for those with larger fractional energy z (Eq. (68)), will be small or even negligible for the following reason: Since Bjorken-x, i.e. the momentum fraction of partons in the nucleon is predominantly small, the d-quark in Fig. 38c (gluon in Fig. 38d) does not have too much momentum in backward direction. This is then even more so for the radiated gluon (pair-produced non-interacting quark) so that its hadron fragments will come out with small fractional energy z in the backward direction or even spill over into the forward hemisphere. Thus at larger z the backward p_T distribution should be dominated by the fragments of the diquark in Fig. 38c (triquark in Fig. 38d) which has $p_T = 0$ as in Fig. 38a. The argument does of course not hold for the forward-going quark (and gluon) in Fig. 38b, since after current absorption it has a large momentum fraction $1-x$ in forward direction. That the backward jet is practically not widened by the processes of Fig. 38c, d has also been confirmed quantitatively by Peccei and Rückl [37].

The factor $\langle z^2 \rangle$ occurs since the two quantities in the square bracket refer to the fragmenting parton and only a fraction of the parton energy is transferred to the hadron. The main W dependence of $\langle p_T^2 \rangle_F$ comes from the QCD term $\langle k_T^{2QCD} \rangle$ which is predicted to be [38, 39]

$$\langle k_T^{2QCD} \rangle \propto \alpha_s(Q^2) \cdot W^2 \propto W^2 / \ln \frac{Q^2}{\Lambda^2} \quad \text{with} \quad W^2 = M^2 + Q^2 \left(\frac{1}{x} - 1 \right). \tag{67}$$

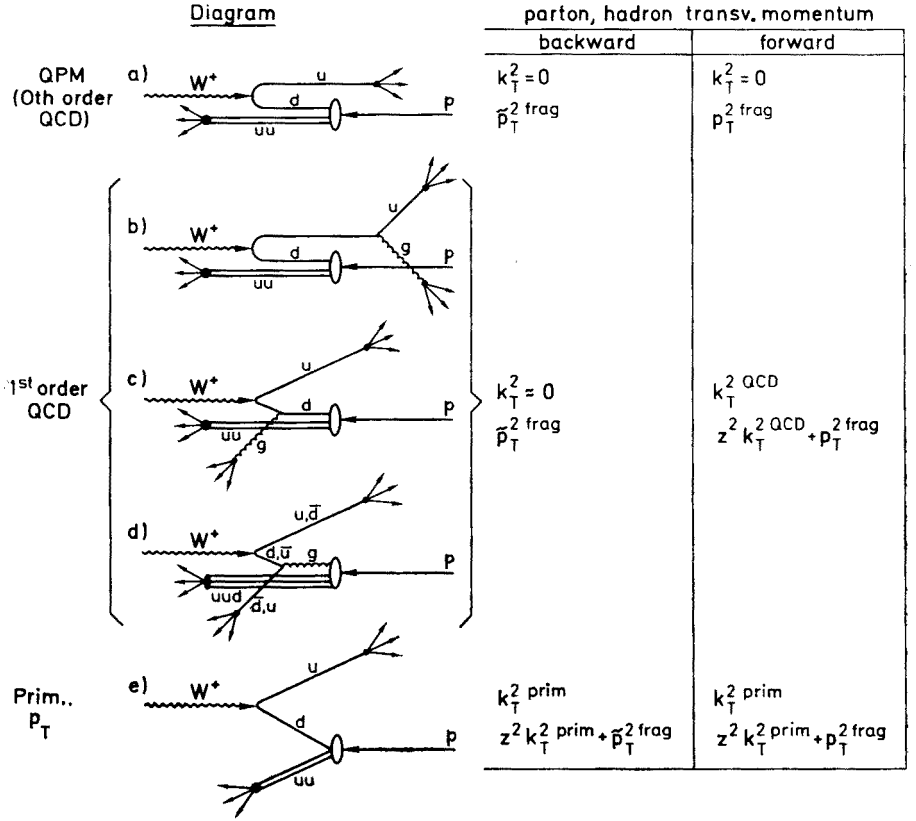

Fig. 38. Processes leading to a transverse momentum of a secondary hadron: (a) fragmentation only, (b) gluon emission after current absorption, (c) gluon emission before current absorption, (d) $q\bar{q}$ pair production from a gluon in the nucleon, (e) primordial p_T of the quark inside the nucleon. On the right hand side, the averaging brackets $\langle\rangle$ are omitted for simplicity

The contribution of the primordial transverse momentum to $\langle p_T^2 \rangle$ is expected to be proportional to z^2 whereas the QCD contribution first rises with z and then drops when $z \to 1$ [37].

1. Results on transverse momentum

We now present the experimental results [40] and discuss them in terms of the ideas explained above and sketched in Fig. 38. To make the forward-backward separation more meaningful, only events with $W > 4$ GeV and $Q^2 > 1$ GeV^2 (3018 CC events)

are considered. Fig. 39 shows $\langle p_T^2 \rangle$ and $\langle p_n^2 \rangle$ vs. W^2, separately for forward hadrons and backward hadrons. It is seen that $\langle p_T^2 \rangle$ increases strongly with W in forward direction, whereas it is less W dependent for the backward going particles. This is in qualitative agreement with a contribution from Fig. 38b and with Eqs. (66), (67). Furthermore, Eq. (65) is rather well fulfilled. On the other hand the Q^2 dependence of $\langle p_T^2 \rangle$ (not shown) is rather weak [12, 40].

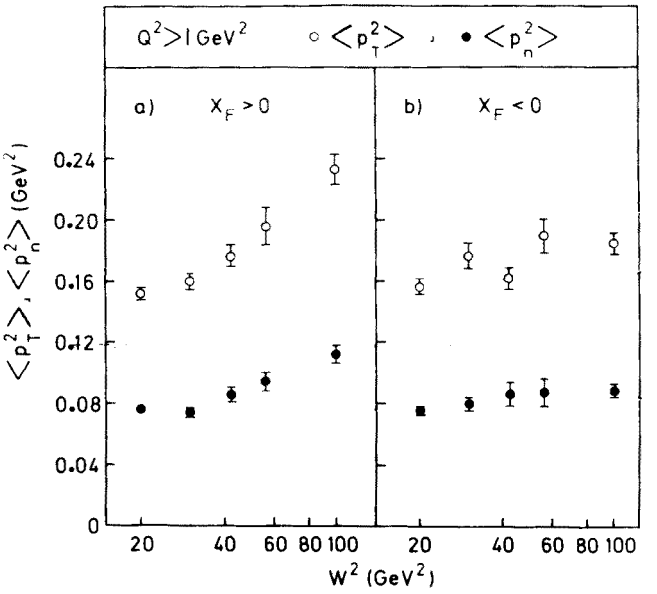

Fig. 39. Average p_T^2 and p_n^2 of hadrons going (a) forward ($x_F > 0$) and (b) backward ($x_F < 0$) in the hadronic cm system vs W^2 in νp scattering

In Fig. 40a $\langle p_T^2 \rangle$ is plotted vs z [11] for two ranges of (low and high) W, separately for the forward and backward hemispheres. (The backward hemisphere is plotted to the left with z replaced by $-z$). Fig. 40b shows the same for $\langle p_n^2 \rangle$ out of the lepton plane. A strong increase of $\langle p_T^2 \rangle$ with z is apparent which is the well-known seagull effect and is expected according to the discussion above. Furthermore at small W ($4 < W < 6$ GeV) a forward-backward symmetry is observed, whereas for large $W > 8$ GeV and $z > 0.3$ $\langle p_T^2 \rangle$ is definitely larger in forward than in backward direction. Thus, $\langle p_T^2 \rangle$ rises with W and z in forward direction. This is also seen in Fig. 41 where $\langle p_n^2 \rangle$ for forward particles is plotted vs. W for fixed intervals of z; the points fall on smooth curves, as indicated by the straight lines. On the other hand, $\langle p_T^2 \rangle$ seems to be rather independent of W for $z \gtrsim 0.3$ in the backward direction. It is obvious that these results are predicted —

[11] In this chapter z is taken as

$$z = \frac{2E^*}{W}, \tag{68}$$

where E^* is the energy of the hadron in the hadronic cm system.

at least qualitatively — if the diagram of Fig. 38b contributes; this prediction should not be much disturbed by the processes of Fig. 38c, d as is explained in the footnote 10.

Can the observed increase of $\langle p_T^2 \rangle$ with W in forward direction be due to other sources? First, it has been checked by a randomisation procedure that the increase does not come

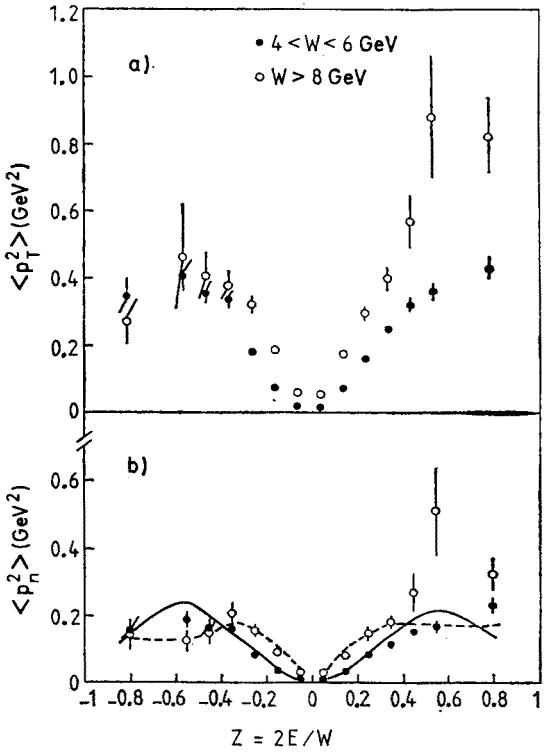

Fig. 40. Average p_T^2 (a) and p_n^2 (b) of hadrons going forward ($z > 0$) and backward ($z < 0$) in the cm system vs energy fraction z, for $4 < W < 6$ GeV and $W > 8$ GeV. The curves are the predictions of longitudinal phase space for $4 < W < 6$ GeV (full curve) and $W > 8$ GeV (dashed curve)

from measurement errors in the hadron momenta or in the muon angle. Furthermore it cannot be explained by longitudinal phase space (LPS) as has been checked by Monte Carlo simulations the results of which are shown by the curves in Fig. 40b (full curve for $4 < W < 6$ GeV, dashed curve for $W > 8$ GeV). Finally the increase could be produced by the opening of a new channel, e.g. for charm production. Let

$$f(z) = \frac{N_n}{N_0} \tag{69}$$

be the ratio of hadrons from the "new" process (with $\langle p_T^2 \rangle_n$) over those from the "old" process (with $\langle p_T^2 \rangle_0$). Then

$$\langle p_T^2 \rangle_{tot} = \frac{\langle p_T^2 \rangle_n N_n + \langle p_T^2 \rangle_0 N_0}{N_n + N_0} . \tag{70}$$

From this one obtains:

$$f(z) = \frac{R(z)-1}{\alpha(z)-R(z)} \tag{71}$$

with

$$R(z) = \frac{\langle p_T^2\rangle_{tot}(z)}{\langle p_T^2\rangle_0(z)} \quad \text{and} \quad \alpha(z) = \frac{\langle p_T^2\rangle_n(z)}{\langle p_T^2\rangle_0(z)} \,. \tag{72}$$

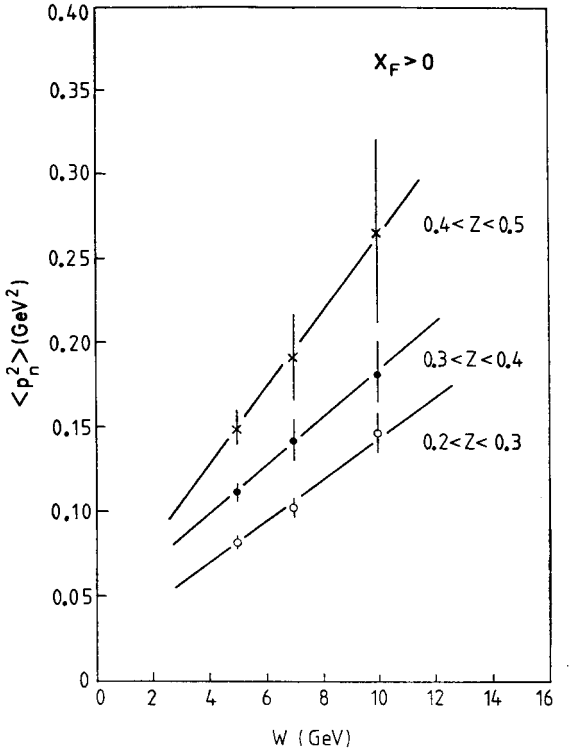

Fig. 41. Average p_n^2 of hadrons going forward in the hadronic cm system vs W for three intervals of the energy fraction z. The straight lines are linear fits to the data points

$\alpha(z)$ can be obtained from charmed-particle decay, $R(z)$ from the data points in Fig. 40 for $4 < W < 6$ GeV ($\langle p_T^2\rangle_0$) and $W > 8$ GeV ($\langle p_T^2\rangle_{tot}$). The resulting value of f (for $\alpha = 2$: $f = 1.7$ for $0.3 < z < 0.4$, $f = 0.7$ for $z > 0.6$) is much too large to be accounted for by charmed particle production. Thus the only reasonable explanation for the increase of $\langle p_T^2\rangle$ seems to be a contribution from hard-gluon bremsstrahlung, Fig. 38b.

If this is the case one may try to isolate the W-dependent QCD part

$$\langle p_T^{2QCD}\rangle \equiv \langle k_T^{2QCD}\rangle \langle z^2\rangle \tag{73}$$

in Eq. (66) from the W-independent non-perturbative part

$$\langle p_T^{2NP}\rangle \equiv \langle k_T^{2prim}\rangle \langle z^2\rangle + \langle p_T^{2frag}\rangle \tag{74}$$

in the following way: If we assume that the QCD effects are negligible in the backward direction and that the diquark fragments in the same way (in particular with the same $\langle z^2 \rangle$) as the single current quark, as seems to be indicated by the forward-backward symmetry in Fig. 40 for small W, then $\langle p_T^{2NP} \rangle$ may be represented by $\langle p_T^2 \rangle_B$ of the backward going particles such that

$$\Delta_1 \langle p_T^2 \rangle \equiv \langle p_T^2 \rangle_F - \langle p_T^2 \rangle_B = \langle p_T^{2QCD} \rangle \tag{75}$$

is the QCD part (analogously for the component p_n). Fig. 42a shows $\Delta_1 \langle p_n^2 \rangle$ as a function of W^2 for $z > 0.2$ together with the QCD prediction (dashed curve) as calculated by Mazzanti

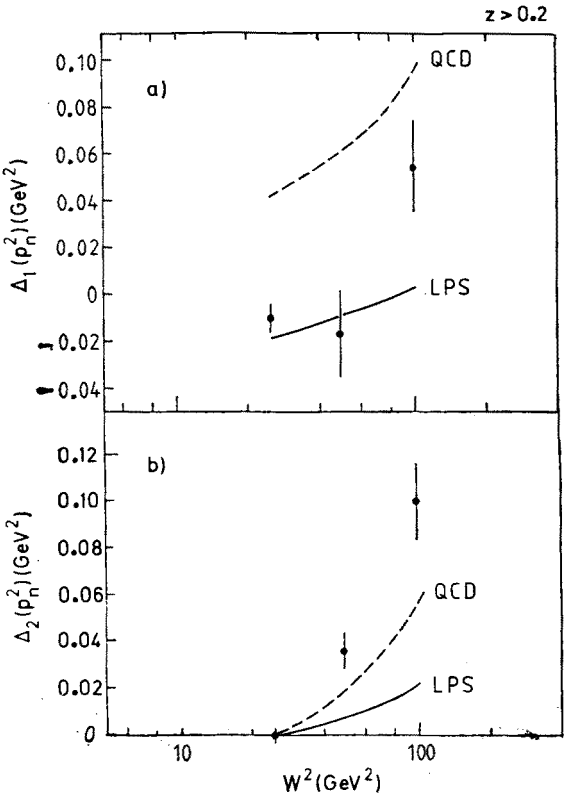

Fig. 42. The differences $\Delta_1 \langle p_n^2 \rangle$ (a) and $\Delta_2 \langle p_n^2 \rangle$ (b) (defined in the text) for hadrons with $z > 0.2$ vs W^2. The curves show the predictions of QCD (dashed) and longitudinal phase space (full)

et al. [41]. The result is rather disappointing; there is no absolute agreement between the data points and theory. This disagreement may be due to the invalidity of the assumption made about the diquark-fragmentation and/or to a non-negligible widening of the backward jet because of the diagrams in Figs. 38c, d such that in Eq. (75) too much is subtracted ($\langle p_T^2 \rangle_B > \langle p_T^{2NP} \rangle$). The prediction of LPS (full curve) seems to be somewhat closer to the data.

A *relative* comparison of the observed W dependence of $\langle p_T^2 \rangle_F$ with theory may be carried out by using the forward information only, i.e. without assumptions about the diquark-fragmentation. Fig. 42b shows for hadrons with $z > 0.2$ the difference

$$\Delta_2 \langle p_n^2 \rangle \equiv \langle p_n^2 \rangle_F(W) - \langle p_n^2 \rangle_F (W = 5 \text{ GeV}) \tag{76}$$

as a function of W both experimentally (points) and theoretically (dashed curve for QCD [41], full curve for LPS). The observed W dependence of this difference is somewhat steeper than predicted by QCD.

2. Search for planar events

Planar three-jet events corresponding to $e^+e^- \to q\bar{q}g$ with three hadron jets in a plane have been observed in e^+e^- annihilation at the high energies ($W = \sqrt{s} \approx 30$ GeV) of PETRA [42]. Such planar events, which eventually at very high W should show a three-jet structure (quark-gluon-diquark) are also expected in νN scattering according to the diagram of Fig. 38b. The question arises, whether events with a planar hadron distribution are present already at the relatively low W values of this experiment. According to the momentum-tensor method developed in Ref. [43] and applied to e^+e^- annihilation in Ref. [42], for each event the momentum tensor

$$M_{\alpha\beta} = \sum_i p_{i\alpha} p_{i\beta} \tag{77}$$

is calculated in the hadronic cms where $p_{i\alpha}$ ($\alpha = x, y, z$) are the momentum components of the ith hadron of the event. Diagonalizing this tensor yields the principal axes $\hat{n}_1, \hat{n}_2, \hat{n}_3$ and the eigenvalues Λ_1, Λ_2, Λ_3, which are normalised as

$$Q_K = \frac{\Lambda_K}{\sum p_i^2} \quad \text{with} \quad Q_1 + Q_2 + Q_3 = 1 \tag{78}$$

and ordered such that

$$0 \leqslant Q_1 \leqslant Q_2 \leqslant Q_3 \leqslant 1. \tag{79}$$

The sphericity S and aplanarity A of the event is then given by

$$S = \tfrac{3}{2}(Q_1 + Q_2),$$
$$A = \tfrac{3}{2} Q_1. \tag{80}$$

For an ideal flat event $Q_1 = 0$, i.e. $A = 0$; for an ideal two-jet event $Q_1 = Q_2 = 0$, i.e. $Q_3 = 1$, $A = 0$, $S = 0$. This means that $\hat{n}_1$ is the normal to the plane of a planar event and $\hat{n}_3 = \hat{S}$ is the sphericity axis with respect to which $\Lambda_3 = \sum_i p_{i\parallel}^2$ is a maximum, i.e. $\sum_i p_{iT}^2$ is a minimum. Thus a planar event is characterized by a small value of A and a large value of S.

A search for planar events in this experiment was carried out using only events with at least six charged hadrons in the final state. Events with low multiplicity are thus eliminated since their track configuration is too strongly restricted by energy-momentum conser-

vation. The results of the search are summarised in Table II where three different cuts in S and A are applied ($S > 0.25$, $A < 0.04$; $S > 0.25$, $A < 0.025$; $S > 0.4$, $A < 0.04$). The first row of the table gives the observed number of events obeying these cuts for three intervals of W. Three different methods were applied to find out if the observed event numbers indicate the presence of real planar events or whether they are just the tails of an "ordinary" particle distribution:

a. Each track of an observed event was rotated by a random angle φ around the current direction $\bar{q}$ in order to destroy by this randomisation procedure any possible planarity in the real event. The quantities S and A were then recomputed for the randomized events and the numbers of events obeying the S and A cuts are given in the second row of Table II.

TABLE II

Results of search for planar events

Selection	$S > 0.25$, $A < 0.04$			$S > 0.25$, $A < 0.025$			$S > 0.4$, $A < 0.04$		
$\langle W \rangle$ (GeV)	5	7	10	5	7	10	5	7	10
Observed	58 ± 8	35 ± 6	26 ± 5	22 ± 5	12 ± 3	12 ± 3	25 ± 5	11 ± 3	3 ± 1.7
Rotation around $\hat{q}$	61	31	25	28	8	12	26	8	5
Rotation around $\hat{S}$	39	24	13	17	6	4	12	3	2
Monte Carlo prediction	82	25	13	38	10	6	36	6.5	1.3

b. Instead of rotating around $\hat{q}$, each track of a real event was randomly rotated around the sphericity axis $\hat{S}$ (thus leaving S unchanged, but changing A), and the same analysis as above was performed. The resulting numbers of events are given in the third row of Table II.

c. Events were generated by the Monte-Carlo program mentioned above, using longitudinal phase space, and the same analysis was carried out with the simulated events. The fourth row of Table II gives the numbers of simulated events obeying the various S and A cuts.

The table shows that there is no relevant excess of observed over expected numbers of events, i.e. there is no significant indication for the presence of planar events corresponding to Fig. 38b at the relatively low values of W in this experiment. The relatively low event numbers obtained with method b. (third row in Table II) are of instrumental origin and are also obtained when the randomisation procedure b. is applied to the Monte-Carlo-generated events.

3. Primordial transverse momentum

As Fig. 38e indicates, the presence of a primordial k_T^{prim} of the quarks in the nucleon leads to an inclination of the direction $\hat{n}$ of the fragmenting quark with respect to the current direction $\hat{q}$. Because of the fragmentation into hadrons, this direction $\hat{n}$ is however not identical with the measured event (sphericity) axis $\hat{S}$, as is easily seen e.g. in the cascade

model for the fragmentation process (in analogy to Fig. 15 for the charges): Since the quarks of the $q\bar{q}$ pairs in the cascading chain have on the average a transverse momentum with respect to the original direction $\hat{n}$, the measured axis $\hat{S}$ is tilted with respect to $\hat{n}$ due to p_T^{frag}.

For each event an angle θ between $\hat{q}$ and $\hat{S}$ and a transverse momentum

$$k'_T = \sin\theta \cdot \sum_i \vec{p}_i \cdot \hat{S} \quad \text{with} \quad \cos\theta = \hat{q} \cdot \hat{S} \tag{81}$$

has been calculated where the sum $\sum_i$ extends over all hadrons with $\vec{p}_i \cdot \hat{S} > 0$. The sum $\sum_i \vec{p}_i \cdot \hat{S}$ gives an estimate of the momentum k_q of the fragmenting quark such that for $\hat{n} = \hat{S}$ k'_T would be the primordial k_T^{prim}. In reality however k'_T has also a contribution

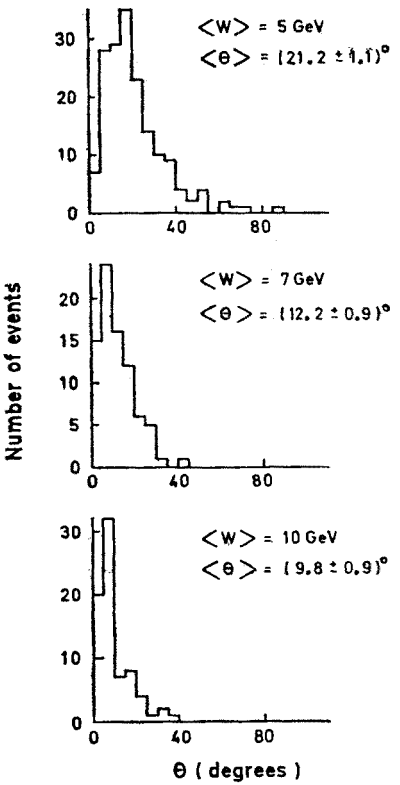

Fig. 43. Distribution of the angle θ between the current direction and sphericity axis for three average values of W

from the fragmentation as explained above such that $\langle k'_T \rangle$ is only an upper limit for $\langle k_T^{prim} \rangle$. An obvious alternative determination of k'_T (without using sphericity explicitly) is given by the formula

$$k'_T = \sin\theta' \cdot |\sum \vec{p}_i|, \tag{82}$$

where θ' is the angle between $\sum \vec{p}_i$ and $\hat{q}$. It should be pointed out that equations (81) and (82) are not changed, if the current quark in Fig. 38e emits a bremsstrahlung gluon before fragmentation since the gluon fragments are and must be included in the procedure to obtain the total momentum of the original current quark after the absorption of the current.

If one omits the unmeasured neutral particles in an event the determination of k'_T is distorted, since with the charged hadrons only, the quark momentum k_q is determined

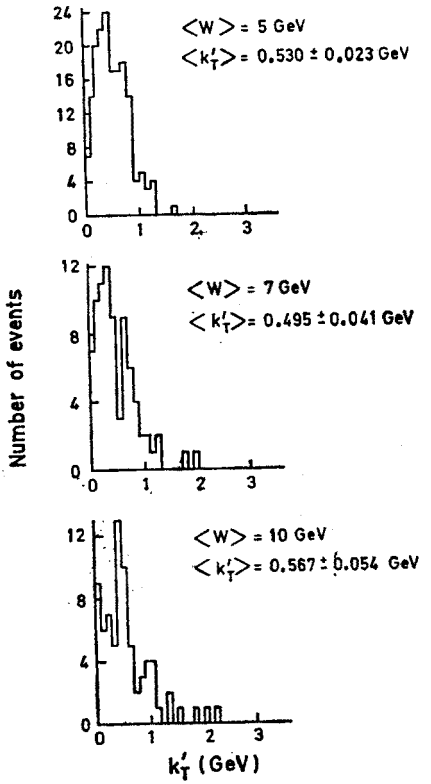

Fig. 44. Distribution of the transverse momentum k'_T, defined by Eq. (81), for three average values of W

incorrectly and the angles θ, θ' may be shifted. Therefore, for the actual analysis only events without neutral hadrons (3C-fits) are used, which amounts to 325 charged-current 3C-events with $Q^2 > 1$ GeV^2, $W > 4$ GeV. Fig. 43 gives the distribution of θ, Fig. 44 the distribution of k'_T, Eq. (81), for three intervals of W. As expected the θ distribution becomes narrower with increasing W (corresponding to the increasing quark momentum k_q) whereas the k'_T distribution is rather independent of W. The average values $\langle\theta\rangle$, $\langle k'_T\rangle$ and $\langle k'^2_T\rangle$ as determined from Eq. (81) are given in Table III in columns A, B, D respectively. Columns C and E of the table give $\langle k'_T\rangle$ and $\langle k'^2_T\rangle$ as obtained by the alternative method, Eq. (82). The differences of the values from the two procedures are a measure of the intrinsic

TABLE III

Estimate of the primordial transverse momentum

$\langle W \rangle$ (GeV)	A $\langle \theta \rangle$ (degr.)	B $\langle k'_T \rangle$ (GeV)	C $\langle k'_T \rangle$ (GeV)	D $\langle k'^2_T \rangle$ (GeV^2)	E $\langle k'^2_T \rangle$ (GeV^2)
5	21.2±1.1	0.530±0.023	0.581±0.025	0.370±0.030	0.440±0.035
7	12.2±0.9	0.495±0.041	0.583±0.038	0.383±0.069	0.456±0.066
10	9.8±0.9	0.567±0.054	0.685±0.057	0.537±0.105	0.713±0.113

uncertainty in determining k'_T. Assuming $\langle p_T^{2\text{frag}} \rangle$ to be in the range 0.12 to 0.20 GeV^2, the primordial $\langle k_T^{2\text{prim}} \rangle$ is found to be of the order 0.25 to 0.35 GeV^2 corresponding to a $\langle k_T^{\text{prim}} \rangle$ between ~0.5 and 0.6 GeV.

It is a great pleasure to thank my colleagues in the ABCMO Collaboration for many fruitful and exciting discussions and the very pleasant cooperation in the collaboration. I thank R. Peccei and R. Rückl for discussions on a theoretical question. Furthermore, I am grateful to my secretary E. Thurner for her careful and diligent work in preparing these lecture notes. I thank W. Wittek for many helpful discussions and for a critical reading of the manuscript. Finally I express my gratitude to my Polish friends for their great hospitality extended to me during my stay in Zakopane.

REFERENCES

[1] C. Brand et al., *Nucl. Instrum. Methods* **136**, 485 (1976).
[2] H. G. Heilmann, Bonn Internal Report WA21-int-1 (1978).
[3] G. Myatt, CERN ECFA Report 72/4, Vol. 2, 117 (1972); A. Grant, *Nucl. Instrum. Methods* **127**, 355 (1975).
[4] J. Blietschau et al., *Phys. Lett.* **86B**, 108 (1979); Proc. Neutrino 79, Bergen, Vol. 2, p. 44 (1979); K. L. Wernhard, Proc. 14th Rencontre de Moriond, Vol. II, p. 359 (1979).
[5] J. Blietschau et al., *Phys. Lett.* **87B**, 281 (1979); Proc. Intern. Conf. High-Energy Phys., Geneva, Vol. 1, p. 151 (1979); Proc. Neutrino 79, Bergen, Vol. 2, p. 499 (1979); W. G. Scott, Proc. 14th Rencontre de Moriond, Vol. I, p. 307 (1979); Proc. Neutrino 79, Bergen, Vol. 2, p. 533 (1979).
[6] J. Blietschau et al., *Phys. Lett.* **88B**, 381 (1979); Proc. Neutrino 79, Bergen, Vol. 2, p. 383 (1979).
[7] J. Blietschau et al., Proc. Neutrino 79, Bergen, Vol. 2, p. 507 (1979).
[8] J. Blietschau et al., Proc. Neutrino 79, Bergen, Vol. 2, p. 515 (1979).
[9] J. Blietschau et al., Proc. X. Intern. Symposium on Multiparticle Dynamics, Goa p. 612 (1979).
[10] D. H. Perkins, Proc. Neutrino 79, Bergen, Vol. 1, p. 429 (1979).
[11] B. Tallini, Proc. Intern. Conf. High-Energy Phys., Geneva, Vol. 1, p. 81 (1979).
[12] N. Schmitz, Proc. Intern. Symp. Lept. Phot. Interactions at High Energies, Fermilab, p. 359 (1979).
[13] D. R. O. Morrison, Proc. 14th Rencontre de Moriond, Vol. II, p. 457 (1979).
[14] H. Harari, E. Rabinovici, *Phys. Lett.* **43B**, 49 (1973); K. Fiałkowski, H. I. Miettinen, *Phys. Lett.* **43B**, 61 (1973); L. Van Hove, *Phys. Lett.* **43B**, 65 (1973); A. Wróblewski, *Acta Phys. Pol.* **B4**, 857 (1973); N. Schmitz, *Acta Phys. Pol.* **B4**, 689 (1973).
[15] J. Whitmore, *Phys. Rep.* **C10**, 273 (1974); **C27**, 187 (1976).
[16] J. Salava, V. Simak *Nucl. Phys.* **B69**, 15 (1974).
[17] E. De Wolf, J. J. Dumont, F. Verbeure, *Nucl. Phys.* **B87**, 325 (1975).
[18] E. Albini et al., *Nuovo Cimento* **32A**, 101 (1976).

[19] W. Thomé et al., *Nucl. Phys.* **B129**, 365 (1977).
[20] S. J. Orfanidis, V. Rittenberg, *Nucl. Phys.* **B59**, 570 (1973); T. Fields et al., Proc. Symp. on Antinucleon-Nucleon Interactions, Liblice-Prague, CERN 74–18, p. 151 (1974).
[21] Z. Koba, H. B. Nielsen, P. Olesen, *Nucl. Phys.* **B40**, 317 (1972).
[22] B. Musgrave, Proc. Neutrino 79, Bergen, Vol. 2, p. 556 (1979).
[23] R. D. Field, R. P. Feynman, *Nucl. Phys.* **B136**, 1 (1978).
[24] G. R. Farrar, J. L. Rosner, *Phys. Rev.* **D7**, 2747 (1973); R. N. Cahn, E. W. Colglazier, *Phys. Rev.* **D9**, 2658 (1974); J. L. Newmeyer, D. Sivers, *Phys. Rev.* **D9**, 2592 (1974); S. J. Brodsky, N. Weiss, *Phys. Rev.* **D16**, 2325 (1977).
[25] J. P. Berge et al., *Phys. Lett.* **91B**, 311 (1980).
[26] P. Bosetti et al., *Nucl. Phys.* **B94**, 21 (1975).
[27] C. Geich-Gimbel, Ph. D. thesis, University of Bonn, Bonn-IR-79-47 (1979).
[28] A. M. Cnops et al., Proc. 13th Rencontre de Moriond, Vol. II, p. 361 (1978).
[29] I. Cohen et al., *Phys. Rev. Lett.* **40**, 1614 (1978).
[30] J. F. Owens, *Phys. Lett.* **76B**, 85 (1978); T. Uematsu, *Phys. Lett.* **79B**, 97 (1978).
[31] G. Altarelli, G. Parisi, *Nucl. Phys.* **B126**, 298 (1977).
[32] I. Hinchliffe, C. H. Llewellyn-Smith, *Nucl. Phys.* **B128**, 93 (1977).
[33] N. Sakai, *Phys. Lett.* **85B**, 67 (1979); see also R. Baier, K. Fey, *Z. Phys.* **C2**, 339 (1979).
[34] G. Altarelli et al., *Nucl. Phys.* **B160**, 301 (1979).
[35] A. J. Buras, K. J. F. Gaemers, *Nucl. Phys.* **B132**, 249 (1978).
[36] E. L. Berger *Z. Phys.* **C4**, 289 (1980); *Phys. Lett.* **89B**, 241 (1980); E. L. Berger, S. J. Brodsky, *Phys. Rev. Lett.* **42**, 940 (1979).
[37] R. D. Peccei, R. Rückl, *Nucl. Phys.* **B162**, 125 (1980), and private communication.
[38] G. Altarelli, Proc. 13th Rencontre de Moriond, Vol. II, p. 395 (1978).
[39] R. Odorico, *Phys. Lett.* **89B**, 89 (1979).
[40] B. Saitta, (Aachen-Bonn-CERN-München-Oxford Collaboration), Paper presented at Moriond 1980.
[41] P. Mazzanti, R. Odorico, V. Roberto, *Phys. Lett.* **81B**, 219 (1979).
[42] D. P. Barber et al., *Phys. Rev. Lett.* **43**, 830 (1979); R. Brandelik et al., *Phys. Lett.* **86B**, 243 (1979); Ch. Berger et al., *Phys. Lett.* **86B**, 418 (1979); W. Bartel et al., *Phys. Lett.* **91B**, 142 (1980).
[43] J. D. Bjorken, S. J. Brodsky, *Phys. Rev.* **D1**, 1416 (1970); S. L. Wu, G. Zobernig, *Z. Phys.* **C2**, 107 (1979).